Table 5 Levels of IL-2, IL-1RA, IP-10, IFN-γ, and IL-10 in QFT-IT supernatants with and without TB-antigen stimulation in nonrecurrence and recurrence groups.

	No stimulation (Nil tubes)[a]		*P* value[b]	Stimulated with TB-antigens (TBAg tubes)[a]		*P* value[b]
	Nonrecurrence $n = 10$	Recurrence $n = 10$		Nonrecurrence $n = 10$	Recurrence $n = 10$	
IL-2						
Month 0	9.55 (4.99–10.00)	9.67 (6.45–11.96)	0.6480	119.59 (71.33–301.01)	87.65 (48.07–147.28)	0.1509
Month 2	9.42 (2.77–9.92)	9.42 (3.67–10.00)	0.7606	108.22 (67.52–199.84)	42.55 (34.23–90.57)	0.0588
Month 7	9.42 (2.59–9.92)	9.67 (2.59–10.00)	0.5656	80.86 (43.25–182.72)	40.26 (20.25–84.47)	0.1124
IL-1RA						
Month 0	383.02 (211.01–590.51)	506.14 (316.64–593.18)	0.4057	783.99 (528.86–1177.69)	920.99 (648.56–1065.19)	0.7624
Month 2	184.74 (115.41–298.36)	267.38 (205.48–469.55)	0.0821	455.26 (220.52–758.45)	406.91 (325.55–593.61)	>0.9999
Month 7	144.68 (120.22–158.43)	252.82 (197.18–306.53)	0.0156	360.04 (130.28–528.86)	328.62 (255.49–690.86)	0.4497
IP-10						
Month 0	6465.02 (3950.00–9531.21)	7291.13 (4614.94–13,068.25)	0.4497	136,362.20 (90,912.67–151,897.60)	86,495.93 (53,311.35–120,082.80)	0.0638
Month 2	5511.37 (2435.73–10,045.31)	7256.33 (5237.79–9094.84)	0.4497	128,971.10 (60,384.23–151,897.60)	38,334.16 (17,740.69–53,528.71)	**0.0072**
Month 7	3823.80 (1085.59–5388.28)	7182.96 (3012.90–14,986.52)	0.1736	106,655.30 (28,361.69–151,897.60)	32,663.32 (17,160.10–102,471.50)	0.1038
IFN-γ						
Month 0	126.01 (99.82–211.41)	124.17 (98.70–154.42)	0.9698	784.28 (387.67–1657.85)	393.75 (278.23–600.60)	0.0696
Month 2	81.33 (66.62–102.40)	102.40 (67.86–123.09)	0.2550	391.68 (217.13–1393.35)	157.00 (136.92–174.37)	**0.0041**
Month 7	86.21 (56.12–94.53)	98.34 (74.93–139.49)	0.1730	266.15 (116.70–590.04)	153.38 (113.18–316.82)	0.5453
IL-10						
Month 0	6.40 (6.12–7.97)	6.82 (6.21–12.49)	0.4267	6.12 (5.86–6.21)	7.13 (6.21–11.84)	0.0443
Month 2	6.12 (6.07–6.21)	6.21 (6.07–12.09)	0.2215	6.07 (5.90–6.12)	6.17 (6.07–6.66)	0.1457
Month 7	6.17 (6.07–6.25)	6.17 (5.86–6.59)	0.9393	6.07 (5.86–6.12)	6.21 (5.86–6.78)	0.1264

QFT-IT: QuantiFERON TB-gold In-tube; TB: tuberculosis; TbAg: tuberculosis-specific antigens; NS: non-significant.

[a] Values (pg/ml) are expressed in median (interquartile range).

[b] Compared between non-recurrent and recurrent groups. The *P* values were obtained by Wilcoxon's rank-sum tests; values in bold and underlined are those remained significant after Bonferroni's correction.

duction from CD4+ T-cells in response to certain TB-specific peptides has been observed in patients with severe pulmonary TB.[29] In such a condition, inhibitory receptors and soluble factors that induce T-cell anergy, such as CTLA-4 and IL-10,[30] contribution of regulatory T (Treg)-cells,[31–34] and compartmentalization of TB antigen-specific T-cells[35] may have played a role in low IFN-γ levels. In our study, however, the extent of pulmonary TB lesions, an indicator of TB severity (data not shown), and IL-10 production at 2 months, a marker of Treg activity, were not different between the two groups. Furthermore, according to the abovementioned mechanisms, IFN-γ levels should have been suppressed before treatment and recovered during effective treatment, contrary to the pattern observed in this study. Difference caused by nonspecific immune suppression that may occur in malnutrition or other states is also unlikely because the amount of nonspecific mitogen-induced IGRA response was not significantly different between the two groups (Fig. 3b).

Although our study provided no direct evidence, the impairment of T-cell memory function at the convalescent stage may have caused both the negative conversion and the low IFN-γ values seen in the IGRA results at 2 months in the recurrence group. Several lines of evidence have demonstrated that antigen-specific IFN-γ-only-secreting effector T cells are predominant in untreated active TB disease and also indicate that when the antigen load decreases after starting treatment, dual IFN-γ/IL-2- or single IL-2-secreting T-cells with more memory-cell characters become more predominant.[27,36–40] In the recurrence group, it is possible that dual IFN-γ/IL-2-secreting or polyfunctional T-cells have failed to expand for unknown reasons, whereas IFN-γ-only-secreting cells have continuously decreased, resulting in a significant reduction in overall IFN-γ production. Indeed, IL-2 induction in QFT-IT tended to be lower parallel with the lower IFN-γ response at 2 months in the recurrence group than in the nonrecurrence group. Further immunological studies on lymphocyte subpopulations would be necessary to elucidate the underlying mechanism.

In addition to the low IFN-γ values at 2 months, the increase in IFN-γ values between 2 and 7 months was also associated with early TB recurrence. A previous study[14] revealed a minor and insignificant increase in IFN-γ levels at 6 months after treatment completion in subjects having recurrence risk. It is well known that the IGRA response is higher in active TB than in latent TB infection despite a large overlap,[41–43] and the cytokine-producing capacity of MTB-specific CD4 and CD8 T-cells is associated with increased bacillary burden.[27,38] Collectively, a slight increase in IGRA responses between 2 and 7 months in the recurrence group may indicate significantly increased bacillary burden in the subclinical stage before recurrence.

Additionally, in the treatment failure group, the tendency for decreased IFN-γ levels at 2 months may not be explained by only change in bacillary burden, because the burden should be considerably higher in the failure group. The similarity in IFN-γ level patterns between recurrence and failure may suggest a common underlying mechanism, possibly the impairment of T-cell function, although the statistical power of our study was not strong enough to analyze this with regard to treatment failure.

IP-10 is a small chemokine expressed by antigen-presenting cells and it is induced by IFN-γ.[44] IP-10-based tests are comparable to the IGRA response[44] in different groups of TB-related subjects, including HIV-uninfected and infected subjects evaluated at the time of TB diagnosis or over time.[45,46] However, our study results are not conclusive about the better indicator among the two.

We did not distinguish reinfection from relapse in this study. However, we assumed that relapse cases are predominant because recurrence occurred during the short follow-up period (16 months). It should be emphasized that our findings cannot be used for the prediction of recurrence, because a variety of individual variations in longitudinal patterns of the IGRA response were observed. Nevertheless, our findings provide additional insights on the clinical relevance of IGRA in TB management. Negative conversion of the IGRA response after 2 months of treatment was not a good sign though it is widely believed to indicate clearance of infection.

The strength of the present study lies in the high proportion of patients completing treatment and active follow-up. However, this study has a few limitations. First, the last IGRA was performed at 7 months of treatment. The magnitude of change in IFN-γ values in the recurrence group may have been larger if the evaluation was performed at a later stage. Second, in our settings, we were unable to study the host immune response in detail so as to elucidate the underlying mechanism.[27,47] Third, diabetes, one of the possible confounding factors for TB recurrence, was not actively screened in our study protocol. However, the frequency of diabetes based on a questionnaire-based interview was relatively low (4.6%) in the study population and nonexistent (0%) in the recurrence group. Therefore, we did not include this factor in the multivariate analysis. Nevertheless, our data showed a negative association between IGRA response and recurrence, which may prompt future studies in this field.

In conclusion, this study showed that the patterns of IGRA responses to TB-specific antigens during treatment differ according to recurrence status and thus may provide insights into the immunological background prior to TB reactivation, a major question in this field.

Financial disclosure

This work was supported by a grant from the Program of Japan Initiative for Global Research Network on Infectious Diseases (J-GRID), Ministry of Education, Culture, Sports, Science and Technology (MEXT), Japan. The funder had no role in study design, data collection and analysis, decision to publish, or preparation of the manuscript.

Acknowledgments

The authors would like to thank Dr. Naoki Ishizuka (National Center for Global Health and Medicine) for his valuable advice on the study design, Dr. Nguyen Phuong Hoang, Dr. Bui Thi Nguyet, Ms. Vu Thi Xuan Thu, Dr. Pham Thu Anh (Hanoi Lung Hospital), Dr. Nguyen Van Hung, Dr. Tran Thi

Bich Thuy (National Lung Hospital), Dr. Phan Thi Minh Ngoc, Ms. Nguyen Thi Ha (NCGM-BMH Medical Collaboration Center), and all the healthcare staff of relevant district TB centers for supporting site implementation.

References

1. WHO. *Global tuberculosis report*. WHO/HTM/TB/2012.6; 2013, http://apps.who.int/iris/bitstream/10665/75938/1/9789241564502_eng.pdf [Date last accessed: November 26].
2. Faustini A, Hall AJ, Perucci CA. Risk factors for multidrug resistant tuberculosis in Europe: a systematic review. *Thorax* 2006; **61**:158–63.
3. Luzze H, Johnson DF, Dickman K, Mayanja-Kizza H, Okwera A, Eisenach K, et al. Relapse more common than reinfection in recurrent tuberculosis 1-2 years post treatment in urban Uganda. *Int J Tuberc Lung Dis* 2013;**17**:361–7.
4. Crampin AC, Mwaungulu JN, Mwaungulu FD, Mwafulirwa DT, Munthali K, Floyd S, et al. Recurrent TB: relapse or reinfection? The effect of HIV in a general population cohort in Malawi. *AIDS* 2010;**24**:417–26.
5. Wang JY, Lee LN, Lai HC, Hsu HL, Liaw YS, Hsueh PR, et al. Prediction of the tuberculosis reinfection proportion from the local incidence. *J Infect Dis* 2007;**196**:281–8.
6. Lambert ML, Hasker E, Van Deun A, Roberfroid D, Boelaert M, Van der Stuyft P. Recurrence in tuberculosis: relapse or reinfection? *Lancet Infect Dis* 2003;**3**:282–7.
7. Walzl G, Ronacher K, Hanekom W, Scriba TJ, Zumla A. Immunological biomarkers of tuberculosis. *Nat Rev Immunol* 2011;**11**:343–54.
8. Andersen P, Doherty TM, Pai M, Weldingh K. The prognosis of latent tuberculosis: can disease be predicted? *Trends Mol Med* 2007;**13**:175–82.
9. Hill PC, Fox A, Jeffries DJ, Jackson-Sillah D, Lugos MD, Owiafe PK, et al. Quantitative T cell assay reflects infectious load of *Mycobacterium tuberculosis* in an endemic case contact model. *Clin Infect Dis* 2005;**40**:273–8.
10. Goletti D, Parracino MP, Butera O, Bizzoni F, Casetti R, Dainotto D, et al. Isoniazid prophylaxis differently modulates T-cell responses to RD1-epitopes in contacts recently exposed to *Mycobacterium tuberculosis*: a pilot study. *Respir Res* 2007; **8**:5.
11. Theron G, Peter J, Lenders L, van Zyl-Smit R, Meldau R, Govender U, et al. Correlation of *Mycobacterium tuberculosis* specific and non-specific quantitative Th1 T-cell responses with bacillary load in a high burden setting. *PLoS One* 2012;**7**: e37436.
12. Katiyar SK, Sampath A, Bihari S, Mamtani M, Kulkarni H. Use of the QuantiFERON-TB Gold In-Tube test to monitor treatment efficacy in active pulmonary tuberculosis. *Int J Tuberc Lung Dis* 2008;**12**:1146–52.
13. Lee SW, Lee CT, Yim JJ. Serial interferon-gamma release assays during treatment of active tuberculosis in young adults. *BMC Infect Dis* 2010;**10**:300.
14. Chee CB, KhinMar KW, Gan SH, Barkham TM, Koh CK, Shen L, et al. Tuberculosis treatment effect on T-cell interferon-gamma responses to *Mycobacterium tuberculosis*-specific antigens. *Eur Respir J* 2010;**36**:355–61.
15. Kobashi Y, Mouri K, Yagi S, Obase Y, Miyashita N, Oka M. Transitional changes in T-cell responses to *Mycobacterium tuberculosis*-specific antigens during treatment. *J Infect* 2009;**58**: 197–204.
16. Hirsch CS, Toossi Z, Vanham G, Johnson JL, Peters P, Okwera A, et al. Apoptosis and T cell hyporesponsiveness in pulmonary tuberculosis. *J Infect Dis* 1999;**179**:945–53.
17. Pai M, Joshi R, Bandyopadhyay M, Narang P, Dogra S, Taksande B, et al. Sensitivity of a whole-blood interferon-gamma assay among patients with pulmonary tuberculosis and variations in T-cell responses during anti-tuberculosis treatment. *Infection* 2007;**35**:98–103.
18. Sahiratmadja E, Alisjahbana B, de Boer T, Adnan I, Maya A, Danusantoso H, et al. Dynamic changes in pro- and anti-inflammatory cytokine profiles and gamma interferon receptor signaling integrity correlate with tuberculosis disease activity and response to curative treatment. *Infect Immun* 2007;**75**: 820–9.
19. Bocchino M, Chairadonna P, Matarese A, Bruzzese D, Salvatores M, Tronci M, et al. Limited usefulness of QuantiFERON-TB Gold In-Tube for monitoring anti-tuberculosis therapy. *Respir Med* 2010;**104**:1551–6.
20. Bugiani M, Bonora S, Carosso A, Piccioni P, Cavallero M, Mondo A, et al. The effect of antituberculosis treatment on interferon-gamma release assay results. *Monaldi Arch Chest Dis* 2011;**75**:215–9.
21. Chiappini E, Fossi F, Bonsignori F, Sollai S, Galli L, de Martino M. Utility of interferon-γ release assay results to monitor anti-tubercular treatment in adults and children. *Clin Ther* 2012; **34**:1041–8.
22. Hang NT, Ishizuka N, Keicho N, Hong LT, Tam DB, Thu VT, et al. Quality assessment of an interferon-gamma release assay for tuberculosis infection in a resource-limited setting. *BMC Infect Dis* 2009;**9**:66.
23. Hang NT, Lien LT, Kobayashi N, Shimbo T, Sakurada S, Thuong PH, et al. Analysis of factors lowering sensitivity of interferon-γ release assay for tuberculosis. *PLoS One* 2011;**6**:e23806.
24. Ringshausen FC, Nienhaus A, Schablon A, Schlösser S, Schultze-Werninghaus G, Rohde G. Predictors of persistently positive *Mycobacterium-tuberculosis*-specific interferon-gamma responses in the serial testing of health care workers. *BMC Infect Dis* 2010;**10**:220.
25. Komiya K, Ariga H, Nagai H, Kurashima A, Shoji S, Ishii H, et al. Reversion rates of QuantiFERON-TB Gold are related to pretreatment IFN-gamma levels. *J Infect* 2011;**63**:48–53.
26. Pai M, Joshi R, Dogra S, Mendiratta DK, Narang P, Dheda K, et al. Persistently elevated T cell interferon-gamma responses after treatment for latent tuberculosis infection among health care workers in India: a preliminary report. *J Occup Med Toxicol* 2006;**1**:7.
27. Millington KA, Innes JA, Hackforth S, Hinks TS, Deeks JJ, Dosanjh DP, et al. Dynamic relationship between IFN-gamma and IL-2 profile of *Mycobacterium tuberculosis*-specific T cells and antigen load. *J Immunol* 2007;**178**:5217–26.
28. Chang KC, Leung CC, Yew WW, Ho SC, Tam CM. A nested case-control study on treatment-related risk factors for early relapse of tuberculosis. *Am J Respir Crit Care Med* 2004;**170**: 1124–30.
29. Goletti D, Butera O, Bizzoni F, Casetti R, Girardi E, Poccia F. Region of difference 1 antigen-specific CD4+ memory T cells correlate with a favorable outcome of tuberculosis. *J Infect Dis* 2006;**194**:984–92.
30. Chappert P, Schwartz RH. Induction of T cell anergy: integration of environmental cues and infectious tolerance. *Curr Opin Immunol* 2010;**22**:552–9.
31. Guyot-Revol V, Innes JA, Hackforth S, Hinks T, Lalvani A. Regulatory T cells are expanded in blood and disease sites in patients with tuberculosis. *Am J Respir Crit Care Med* 2006; **173**:803–10.
32. Pang H, Yu Q, Guo B, Jiang Y, Wan L, Li J, et al. Frequency of regulatory T-cells in the peripheral blood of patients with pulmonary tuberculosis from Shanxi province, China. *PLoS One* 2013;**8**:e65496.
33. Hougardy JM, Place S, Hildebrand M, Drowart A, Debrie AS, Locht C, et al. Regulatory T cells depress immune responses to protective antigens in active tuberculosis. *Am J Respir Crit Care Med* 2007;**176**:409–16.

34. Chiacchio T, Casetti R, Butera O, Vanini V, Carrara S, Girardi E, et al. Characterization of regulatory T cells identified as CD4(+)CD25(high)CD39(+) in patients with active tuberculosis. *Clin Exp Immunol* 2009;**156**:463–70.
35. Rahman S, Gudetta B, Fink J, Granath A, Ashenafi S, Aseffa A, et al. Compartmentalization of immune responses in human tuberculosis: few CD8+ effector T cells but elevated levels of FoxP3+ regulatory t cells in the granulomatous lesions. *Am J Pathol* 2009;**174**:2211–24.
36. Sester U, Fousse M, Dirks J, Mack U, Prasse A, Singh M, et al. Whole-blood flow-cytometric analysis of antigen-specific CD4 T-cell cytokine profiles distinguishes active tuberculosis from non-active states. *PLoS One* 2011;**6**:e17813.
37. Casey R, Blumenkrantz D, Millington K, Montamat-Sicotte D, Kon OM, Wickremasinghe M, et al. Enumeration of functional T-cell subsets by fluorescence-immunospot defines signatures of pathogen burden in tuberculosis. *PLoS One* 2010;**5**:e15619.
38. Day CL, Abrahams DA, Lerumo L, Janse van Rensburg E, Stone L, O'rie T, et al. Functional capacity of *Mycobacterium tuberculosis*-specific T cell responses in humans is associated with mycobacterial load. *J Immunol* 2011;**187**:2222–32.
39. Petruccioli E, Petrone L, Vanini V, Sampaolesi A, Gualano G, Girardi E, et al. IFNγ/TNFα specific-cells and effector memory phenotype associate with active tuberculosis. *J Infect* 2013; **66**:475–86.
40. Biselli R, Mariotti S, Sargentini V, Sauzullo I, Lastilla M, Mengoni F, et al. Detection of interleukin-2 in addition to interferon-gamma discriminates active tuberculosis patients, latently infected individuals, and controls. *Clin Microbiol Infect* 2010;**16**:1282–4.
41. Chee CB, Barkham TM, Khinmar KW, Gan SH, Wang YT. Quantitative T-cell interferon-gamma responses to *Mycobacterium tuberculosis*-specific antigens in active and latent tuberculosis. *Eur J Clin Microbiol Infect Dis* 2009;**28**:667–70.
42. Higuchi K, Harada N, Fukazawa K, Mori T. Relationship between whole-blood interferon-gamma responses and the risk of active tuberculosis. *Tuberc (Edinb)* 2008;**88**:244–8.
43. Ling DI, Pai M, Davids V, Brunet L, Lenders L, Meldau R, et al. Are interferon-γ release assays useful for diagnosing active tuberculosis in a high-burden setting? *Eur Respir J* 2011;**38**: 649–56.
44. Ruhwald M, Aabye MG, Ravn P. IP-10 release assays in the diagnosis of tuberculosis infection: current status and future directions. *Expert Rev Mol Diagn* 2012;**12**:175–87.
45. Vanini V, Petruccioli E, Gioia C, Cuzzi G, Orchi N, Rianda A, et al. IP-10 is an additional marker for tuberculosis (TB) detection in HIV-infected persons in a low-TB endemic country. *J Infect* 2012;**65**:49–59.
46. Kabeer BS, Raja A, Raman B, Thangaraj S, Leportier M, Ippolito G, et al. IP-10 response to RD1 antigens might be a useful biomarker for monitoring tuberculosis therapy. *BMC Infect Dis* 2011;**11**:135.
47. Caccamo N, Guggino G, Joosten SA, Gelsomino G, Di Carlo P, Titone L, et al. Multifunctional CD4(+) T cells correlate with active *Mycobacterium tuberculosis* infection. *Eur J Immunol* 2010;**40**:2211–20.

nature genetics

Evolutionary history and global spread of the *Mycobacterium tuberculosis* Beijing lineage

Matthias Merker[1], Camille Blin[2,3], Stefano Mona[2,3], Nicolas Duforet-Frebourg[4], Sophie Lecher[5–8], Eve Willery[5–8], Michael Blum[4], Sabine Rüsch-Gerdes[9], Igor Mokrousov[10], Eman Aleksic[11], Caroline Allix-Béguec[12], Annick Antierens[13], Ewa Augustynowicz-Kopeć[14], Marie Ballif[15], Francesca Barletta[16], Hans Peter Beck[17], Clifton E Barry III[18], Maryline Bonnet[19], Emanuele Borroni[20], Isolina Campos-Herrero[21], Daniela Cirillo[20], Helen Cox[22], Suzanne Crowe[11,23,24], Valeriu Crudu[25], Roland Diel[26], Francis Drobniewski[27,28], Maryse Fauville-Dufaux[29], Sébastien Gagneux[17], Solomon Ghebremichael[30], Madeleine Hanekom[31], Sven Hoffner[32], Wei-wei Jiao[33], Stobdan Kalon[34], Thomas A Kohl[1], Irina Kontsevaya[35], Troels Lillebæk[36], Shinji Maeda[37], Vladyslav Nikolayevskyy[27,28], Michael Rasmussen[36], Nalin Rastogi[38], Sofia Samper[39], Elisabeth Sanchez-Padilla[19], Branislava Savic[40], Isdore Chola Shamputa[18], Adong Shen[33], Li-Hwei Sng[41], Petras Stakenas[42], Kadri Toit[43], Francis Varaine[44], Dragana Vukovic[40], Céline Wahl[12], Robin Warren[31], Philip Supply[5–8,12,46], Stefan Niemann[1,45,46] & Thierry Wirth[2,3,46]

***Mycobacterium tuberculosis* strains of the Beijing lineage are globally distributed and are associated with the massive spread of multidrug-resistant (MDR) tuberculosis in Eurasia. Here we reconstructed the biogeographical structure and evolutionary history of this lineage by genetic analysis of 4,987 isolates from 99 countries and whole-genome sequencing of 110 representative isolates. We show that this lineage initially originated in the Far East, from where it radiated worldwide in several waves. We detected successive increases in population size for this pathogen over the last 200 years, practically coinciding with the Industrial Revolution, the First World War and HIV epidemics. Two MDR clones of this lineage started to spread throughout central Asia and Russia concomitantly with the collapse of the public health system in the former Soviet Union. Mutations identified in genes putatively under positive selection and associated with virulence might have favored the expansion of the most successful branches of the lineage.**

M. tuberculosis and the other members of the *M. tuberculosis* complex (MTBC) remain the leading bacterial killers worldwide and still account for 1.3 million deaths annually[1]. Of major concern is the uncontrolled spread of MDR tuberculosis (defined by resistance to at least the 2 major first-line drugs isoniazid and rifampicin) in regions such as southern Africa[2] and across large Eurasian territories encompassing the Baltic countries, Russia and the 11 other current or former members and participating states of the Commonwealth of Independent States. These countries are all ranked among the 27 countries with a high MDR tuberculosis burden[1].

The massive spread of MDR tuberculosis in Eurasia is predominantly driven by *M. tuberculosis* clones of the Beijing/East Asian lineage[3–6]. Strains from the Beijing lineage have also been associated with large MDR tuberculosis outbreaks elsewhere[7] and appear to be rapidly expanding in population size in settings with contrasting tuberculosis incidence levels[8,9]. Strains of this lineage have been proposed to possess selective advantages in comparison to strains from other MTBC lineages, comprising an increased capacity to acquire drug resistance, linked to hypermutability[10] or the presence of compensatory mutations mitigating the fitness cost of resistance-conferring mutations[11,12], increased transmissibility, hypervirulence and/or more rapid progression to disease after infection[13–17]. However, the association of Beijing strain infection with MDR tuberculosis and/or with specific pathobiological or epidemiological manifestations is not systematic[18]. This heterogeneity suggests the existence of substantial intralineage biogeographical diversity, affecting pathobiological properties.

To investigate this hypothesis, we analyzed the global biogeographical structure and origin of the Beijing branch of the MTBC by standard genotyping of 4,987 clinical isolates from 99 countries linked to drug resistance. In addition, we analyzed the genome sequences of 110 isolates representing the main clonal complexes (CCs) identified to further explore the evolutionary history of this important lineage.

RESULTS

Global biogeographical structure

Our collection of 4,987 isolates from 99 countries (**Supplementary Fig. 1**) represents by far the largest Beijing lineage data set ever

A full list of author affiliations appears at the end of the paper.

Received 21 July 2014; accepted 19 December 2014; published online 19 January 2015; doi:10.1038/ng.3195

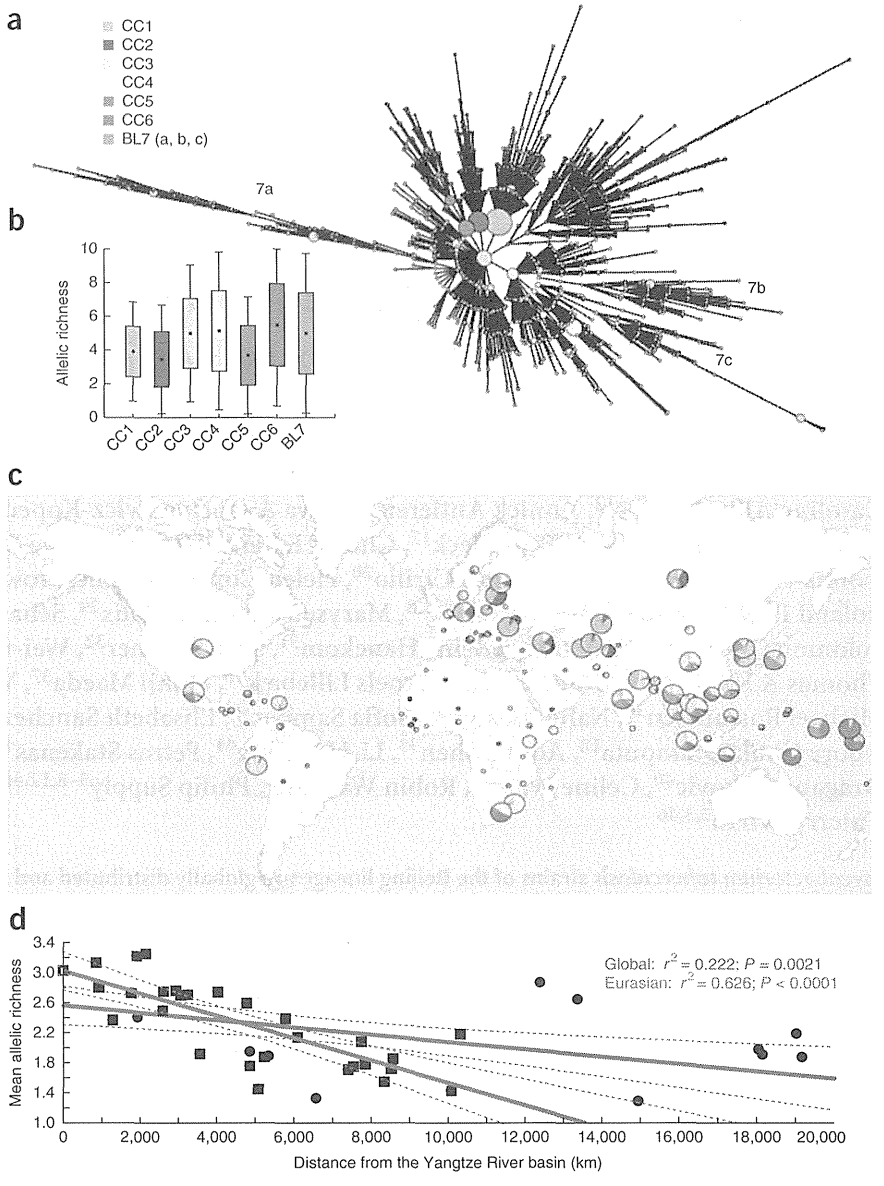

Figure 1 Biogeographical structure of the *M. tuberculosis* Beijing lineage. (**a**) MSTREE based on 24 MIRU-VNTR markers delineating the clonal complexes (CCs) gathered from a worldwide collection ($n = 4,987$). Major nodes and associated multi-locus variants were grouped into six CCs and a basal sublineage (BL). (**b**) Genetic variability in the different Beijing lineage CCs and the BL calculated using a rarefaction procedure (each CC included a subsample of 457 strains drawn randomly from its source population). Dots correspond to the mean allelic richness, boxes correspond to mean values ± s.e.m. and error bars correspond to mean values ± s.d. (**c**) Worldwide distribution of the Beijing CCs and BL. Each circle corresponds to a country, and circle sizes are proportional to the number of strains. Note that the results for CC3 and CC4, less supported by whole genome–based analysis, are only given as an indication. (**d**) Genetic erosion out of China. Mean allelic richness within geographical populations is plotted against geographical distance from the Yangtze River basin. Filled squares denote the Eurasian samples used for the regression; filled circles correspond to the global collection. Confidence intervals are represented by dashed lines.

analyzed in terms of sample size and geographical coverage. Among these, 4,024 isolates (81%) originated from population-based or cross-sectional studies. Beijing strains were detected by screening for typical spoligotypes and best matching of 24-locus mycobacterial interspersed repetitive unit–variable-number tandem repeat (MIRU-VNTR) genotypes obtained from all the isolates[15,19] (**Supplementary Tables 1** and **2**). To gain insight into the global population structure, we constructed a minimum-spanning tree (MSTREE) on the basis of the 24-locus MIRU-VNTR data that minimized the weights of the edges between genotypes. We initially classified the 4,987 isolates into 6 major CCs and 3 distant branches (a, b and c) collectively designated as basal sublineage 7 (BL7) (**Fig. 1a**). PCR analysis of the NTF region[20] of 337 selected isolates showed that CC1–CC5 comprised typical/modern Beijing strains, whereas CC6 and BL7 comprised atypical ancestral Beijing variants (**Supplementary Fig. 2** and **Supplementary Table 3**). We further analyzed the global distributions of CC1, CC2 and CC5, as the corresponding groupings were largely supported (with few to no outliers) by genome sequencing results. Likewise, the ancestral classification of CC6 and BL7 was confirmed by their deep branching in the genome-based trees.

In the MSTREE (**Fig. 1a**), CC1 and CC2, and to a lesser extent CC5, displayed a star-like shape typical of expanding populations, with high-frequency central genotypes surrounded by diffusing layers of variants. Such patterns were much less visible for CC6 and BL7, again suggesting more ancient populations and/or milder expansions. In accordance with this hypothesis, the mean allelic richness (number of alleles), calculated after correcting for sample size effects[21] and taken as a surrogate indication of diversification time, was higher for CC6 and BL7 than for CC1, CC2 and CC5 ($P < 0.05$; **Fig. 1b**).

The spatial distribution on a worldwide scale of these CCs clearly shows a biogeographical structure and population clines in the Beijing lineage (**Fig. 1c**). Strikingly, the CC distribution was the most diverse in the East Asia and Far East region, suggesting that this region indeed represents the origin from which Beijing strains subsequently radiated. The gradient observed in CC5 proportions toward the Pacific Ocean suggests an eastward spread of this clone, followed by successive bottlenecks increasing its frequency in Micronesia and Polynesia. Likewise, we observed westward clines for CC1 and CC2, with these groups becoming highly dominant in central Asia and around the Black Sea (CC1) and in Russia and Eastern Europe (CC2) (**Supplementary Figs. 3** and **4**). In contrast, CC6 and BL7 were more confined to eastern Asia. The only other region where we retrieved substantial proportions of CC6 and BL7 was North America/Mexico, where the CC frequencies resembled those for Chinese samples (**Supplementary Fig. 3**), likely reflecting the effect of recent Chinese immigration.

East Asian origin, multiple epidemic waves and timing

The East Asian origin of the Beijing lineage was further supported by plotting MIRU-VNTR allelic diversity per geographical population

Table 1 MIRU-based demographic and dating estimates of the CCs and lineages detected in the Beijing clade

Clonal complex	N_0^a	N_1^a	$r = N_0/N_1$	t_a^b	TMRCA[b]
CC1	13.106 (7.996–24.713)	0.743 (0.502–1.012)	17.639	263 (190–398)	4,415 (2,569–7,509)
CC2	8.633 (3.954–27.534)	0.529 (0.337–0.856)	16.319	216 (138–350)	1,797 (958–3,690)
CC3	47.204 (32.510–72.062)	1.247 (0.947–1.745)	37.854	559 (445–719)	3,151 (1,750–5,801)
CC4	32.830 (24.125–46.892)	1.683 (1.247–2.362)	19.507	699 (523–928)	4,084 (2,616–6,764)
CC5	8.465 (4.905–18.015)	0.581 (0.394–0.882)	14.570	240 (164–360)	1,492 (872–2,898)
CC6	66.439 (47.548–97.318)	2.609 (2.004–3.559)	25.465	1,226 (967–1,552)	6,161 (3,419–10,725)
BL7	22.864 (17.939–29.514)	3.030 (2.349–4.147)	7.546	1,398 (1,056–1,834)	5,212 (3,613–8,962)
Global lineage[c]	67.098 (54.007–86.504)	3.053 (2.331–4.160)	21.978	1,275 (1,007–1,613)	6,604 (4,270–12,514)

N_0, current effective population size; N_1, ancestral population size prior expansion; t_a, time elapsed since the last expansion began; TMRCA, time to the most recent common ancestor.

[a]Effective population sizes are expressed in millions. [b]Datings are expressed in years. Estimates correspond to the median values, and numbers in parentheses correspond to the 95% highest posterior density (HPD) intervals generated during the Bayesian analysis. [c]Estimates based on 10 reiterations following a subsampling procedure of 500 strains from the full data set (±s.d.).

against geographical distance from the Yangtze River basin (**Fig. 1d**). Allelic diversity decreased with increasing geographical distance, and 22% of the variance could be explained by geography alone when considering the full data set. Interestingly, this percentage increased to 63% when focusing solely on the Eurasian samples. This difference reflects the excess of allelic richness in the samples collected, especially in North America and in South Africa, likely resulting from substantial recent immigration from China.

We then attempted to date past expansions and to generate estimates for the time to the most recent common ancestor (TMRCA). Because it is not possible to simultaneously estimate N (the effective population size) and μ (the mutation rate), we implemented mutation rate priors and intervals covering previously reported μ values[22–24] (**Supplementary Fig. 5**). By applying these rates and a generation time of 1 d for *M. tuberculosis*, we estimated a mean TMRCA of 6,600 years for the Beijing lineage (**Table 1**). According to coalescent analyses, CC6 and BL7 are the two oldest sublineages, with TMRCAs of ~6,000 and 5,000 years, respectively, and CC5 is the youngest, with a TMRCA of ~1,500 years.

Genetic data can also be used to unravel recent demographic changes. By using Bayesian-based coalescent tools available for VNTR markers, we tested whether a recent decline or increase in bacterial population size occurred and calculated t_a, reflecting the time elapsed since a last expansion began. All CCs displayed strong expansion signatures (**Table 1**). The expansion ratio $r = N_0/N_1$ (where N_0 is the current effective population size and N_1 is the effective population size before expansion began) ranged from 8 (BL7) to 25 (CC6). For CC1, CC2 and CC5, the expansion onset, provided by median t_a values, dated back some 200–250 years. These findings clearly contrast with the much older expansions detected for CC6 and BL7 dating back to the medieval period (**Table 1**).

Whole genome–based phylogeny and recent population dynamics

Because MIRU-VNTR loci may be affected by homoplasy[25], we sequenced the genomes of 110 strains (**Supplementary Fig. 6** and **Supplementary Table 4**) representing the 7 sublineages initially identified by genotyping to obtain a robust tree topology and confirm the ancestral clades. After removing genes associated with drug resistance, repetitive and mobile elements, and artifactual SNPs linked to indels[26], we detected 6,001 polymorphic sites (SNPs). Likelihood mapping analyses[27] indicated a robust phylogenetic signal (>81%), albeit with minor occurrence of star-likeness, signaling that the tree was well resolved in certain parts only (**Supplementary Fig. 7**). In contrast to a recent report suggesting some degree of horizontal gene transfer (HGT) in the MTBC[28], analysis of neighbor nets and densitrees identified no major splits suggestive of HGT (**Supplementary Figs. 8** and **9a**), and the pairwise homoplasy index (PHI) test did not find evidence ($P = 0.7668$) for recombination that might blur phylogenetic reconstruction. The genome-based tree topology was fully consistent with Beijing linage–specific regions of difference (RD181 and RD150). Numerous subgroup-specific polymorphisms also clearly distinguished three ancestral and five modern Beijing phylogenetic clades (**Fig. 2a**, **Supplementary Fig. 9b** and **Supplementary Table 5**), fairly congruent with the MIRU-VNTR groupings except for CC3 and CC4 (**Fig. 2a**). Strains associated with BL7 clearly corresponded to the most ancestral population, followed by CC6 strains. As such, we refer to both groups as Asian ancestral subgroups 1–3. Strains from the modern CCs diverged more recently and displayed shorter branches. Central Asian, European-Russian and Pacific branches also largely confirmed the CC1, CC2 and CC5 classifications, respectively. However, CC4 strains could be clearly differentiated into two genome-based subgroups (Asian Africa 1 and 2), whereas the distribution of CC3 isolates was much more scattered on the tree. This partial incongruence in the MIRU-VNTR–based tree likely reflects homoplastic effects and/or hard polytomies in the context of recent expansions.

Genome-wide SNP information provides the potential for more sensitive detection of one or even several population changes. However, such analysis requires calibration of the genome evolution rate, which is not trivial. Confident, closely matching estimates of short-term genome mutation rates, ranging between 1.0×10^{-7} and 1.3×10^{-7} substitutions per nucleotide site per year, have been independently obtained from the study of different contemporary epidemics[26,29] and a macaque infection model[30]. However, such estimates are supposed to differ by one or two orders of magnitude from the long-term fixation rate, as less fit mutations are purged from the genomic pools[31]. Consequently, if the mutation rate changes through time, any mutation rate used will imply information distortion at some point. Therefore, we decided to use the previously estimated short-term rate of 1×10^{-7} substitutions per nucleotide site per year (95% confidence interval of 0.6×10^{-7} to 1.5×10^{-7})[29] to depict a more likely demographic scenario over the last few hundred years.

We generated a Bayesian skyline plot that estimated changes in the pathogen's effective population size over time (**Fig. 2b**) on the basis of the 110 genomes. We detected a stepping stone–like increase in population size with two sharp population growth phases, one occurring during the Industrial Revolution and the second approximately matching the period of the First World War. It was also striking that the only decrease in population observed on the skyline plot coincided with the onset of large-scale antituberculosis drug use. Although a cumulative effect cannot be excluded (also due to changes, for example,

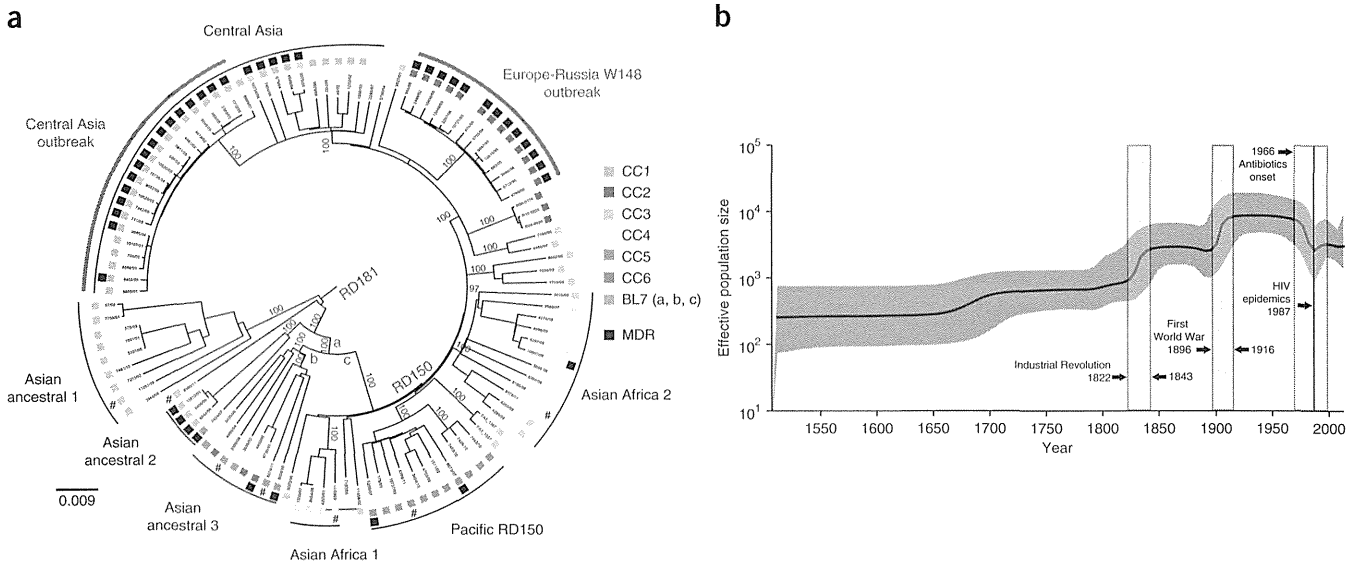

Figure 2 Phylogenetic reconstruction of the MTBC Beijing lineage and change in population size through time. (**a**) Midpoint-rooted maximum-likelihood tree based on 110 genomes and a total of 6,001 concatenated SNPs. Characteristic mutations differentiating modern and ancestral Beijing strain types are mapped on the tree—*mutT4* encoding p.Arg48Gly (branch a), *ogt* encoding p.Arg37Leu (branch b) and *mutT2* encoding p.Gly58Arg (branch c)—as is the absence of the RD181 and RD150 regions of difference. Black squares correspond to strains with an MDR or extremely multidrug-resistant (XDR) phenotype, and a number sign indicates strains lacking drug susceptibility test information. Numbers on branches correspond to bootstrap values. The tree topology remains the same when H37Rv is used as an outgroup. (**b**) Bayesian skyline plot indicating changes in the Beijing lineage over time with a relaxed molecular clock set at 1×10^{-7} mutations per nucleotide per year. The shaded area represents the 95% confidence intervals, and the green colored boxes represent major socioeconomic events that might have affected the demography of *M. tuberculosis*.

in living conditions), we do not favor a major influence from BCG vaccination, whose widespread use started earlier (in the late 1940s) and had a relatively moderate protective effect against tuberculosis[32]. Finally, a temporary reversal of this downward trend was noticeable. Interestingly, this late, mild bacterial expansion matched with the beginning of the HIV epidemics and the first large MDR tuberculosis outbreaks in the former Soviet Union[33] and the United States[34] in the 1990s.

Specific antibiotic resistance

To investigate a possible association between antibiotic resistance and the identified CCs, we examined a subset of 1,054 clinical isolates with known drug resistance profiles from our global strain collection (**Supplementary Table 6**). Of these, 91% (965/1,054) originated from 12 different study settings that were population based or cross-sectional. We avoided including local MDR tuberculosis cohorts. The analysis showed that CC2 had the highest proportion of MDR strains (75.0%, 111/148; $P < 0.0001$) (**Fig. 3**). CC5 as well as the more heterogeneous CC3 and CC4 exhibited the lowest percentages of resistance ($P < 0.01$), with 3.5% (2/57), 12.1% (20/165) and 17.2% (32/186), respectively. Although the proportions of MDR isolates were similar for the modern CC1 (30.4%, 89/293) and the ancestral CC6 (37.7%, 26/69) and BL7 (32.4%, 44/136), the clustering rates (defined as the proportions of isolates with an identical MIRU-VNTR haplotype) of the MDR strains differed significantly ($P < 0.0001$) (**Supplementary Table 7**). In CC1, 94.4% (84/89) of all MDR isolates were associated with a shared MIRU-VNTR haplotype, in comparison to only 42.3% (11/26) and 56.8% (25/44) in CC6 and BL7, respectively (**Supplementary Table 7**). Overall, CC1 and CC2 had the highest clustering rates for MDR strains ($P < 0.01$), indicating population expansion amplified by the recent transmission of MDR strains, especially associated with MIRU-VNTR haplotypes termed 94-32 (CC1) and 100-32 (CC2) according to a standard nomenclature[19].

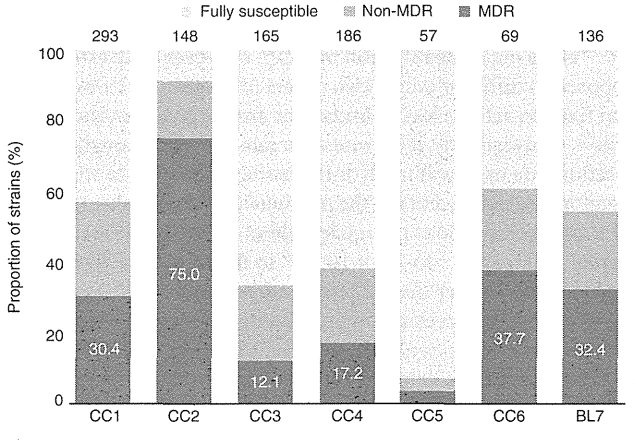

Figure 3 Proportions of MDR tuberculosis strains among the six CCs and BL of the Beijing lineage. Note that CC2 comprises significantly ($P < 0.001$) more MDR strains than the other complexes. The total number of strains with available drug susceptibility test information in each group is given above the corresponding column.

This MDR outbreak hypothesis was strongly supported by the analysis of mean pairwise genetic distances among strain genomes. Strains from the central Asian outbreak (associated with CC1) and from the European-Russian W148 branch (associated with CC2 and defined as a Russian successful clone[6]) exhibited a lower pairwise distance than all other subgroups ($P < 0.05$), with respective means of only 17 and 23 SNPs differentiating pairs of isolates (**Supplementary Fig. 10**). These strains were all resistant to at least isoniazid and streptomycin (with resistance conferred by mutations to *katG* (encoding p.Ser315Thr) and *rpsL* (encoding p.Lys43Arg), respectively; data not shown). These data thus indicate a specific recent expansion of two MDR clones in Russia and central Asia.

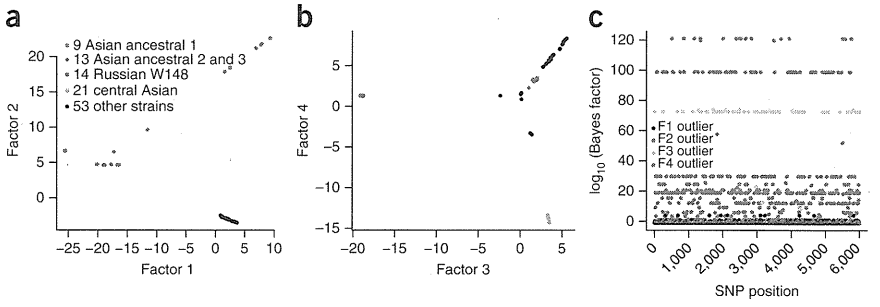

Figure 4 SNP-based Bayesian factor model analysis for detecting genes involved in positive selection in the Beijing lineage. (**a**,**b**) Latent factors of the 6,001 SNPs and 110 strains with the first 2 factors (**a**) and the 2 consecutive ones (**b**). (**c**) Manhattan plot representing the selection scan and the outliers that are related to the different latent factors.

Traces of positive selection

To identify genetic targets potentially linked with the expansion of modern Beijing subgroups some 200–700 years ago (**Table 1**), we first examined 81 polymorphisms characteristic for all modern strains (**Supplementary Table 8**). Among these, we found four and three SNPs in the *mce* (mammalian cell entry) and *vapBC* (virulence-associated protein) gene families, respectively. Moreover, SNPs in the coding regions of the same two gene families were fixed in the genomes of both modern and ancestral Beijing subgroups (**Supplementary Table 5**), possibly suggesting positive selection acting on these genes. To test this hypothesis, we calculated the mutation rates per base pair and the dN/dS ratios (global ratios of nonsynonymous to synonymous SNPs) of the concatenated gene sequences for these two gene families and compared them with corresponding values for essential and non-essential genes, genes encoding polymerases, ribosomal proteins, T cell antigens and lipoproteins, and the *fad* gene family (**Supplementary Table 9**). Within the limits imposed by the low levels of total variation, we found a two- to threefold increase in mutation rate, as well as higher dN/dS values in modern subgroups (0.91–1.83) for *mce* and *vapBC* genes than for any control set (0.26–1.07) (**Supplementary Table 9**). There were also more ($P < 0.05$) amino acid substitutions among the *mce* and *vapBC* gene products than in the control sets in modern subgroups, a situation not encountered in the ancestral subgroups (**Supplementary Table 10**).

Furthermore, we searched for branch-specific SNPs and small deletions that were potential candidates for specific adaptation. Noteworthy among these was a frameshift mutation in *kdpD* (c.2541_2542delCA) specific to all European-Russian W148 MDR outbreak strains, predicted to result in an altered C terminus of the sensor and its fusion to the cognate regulator of the two-component system encoded by the *kdpDE* operon (**Supplementary Table 5**). A partial deletion of the *kdpDE* operon in *M. tuberculosis* has already been associated with greater virulence[35]. We refined the search by performing a genome scan analysis, using a Bayesian model[36] that detects the structure and clustering of individuals in a population, with latent variables called factors. We thereby both inferred population structure and identified 200 'outlier' SNPs, defined as those most related to the detected structure, which were distinguished from noise-containing SNPs. Inspection of the factors (**Fig. 4**) indicated that factor 2 distinguishes the ancestral strains from the derived ones, whereas factors 3 and 4 differentiate, respectively, the European-Russian and central Asian lineages from the other strains. Remarkably, the SNPs with the largest Bayes factors within a factor were found to be concentrated among highly plausible gene targets under positive selection (encoding drug resistance, virulence and surface-exposed proteins) (**Supplementary Table 11**). For factor 2, nonsynonymous SNPs affecting the bulk of the modern strains were found, for instance, in *lysX* (a gene required for resistance to cationic antimicrobial peptides[37]), *fadD28* (encoding a virulence factor[38]) and *mutT2* (a putative mutator gene[39]) (**Supplementary Table 11**). For factor 3, nonsynonymous mutations were found in *pks5* (involved in the biosynthesis of surface-exposed polyketides[40]), *mce3B* (encoding an invasin-adhesin–like protein[41]) and *Rv1877* (involved in efflux pump–mediated drug resistance in *Mycobacterium smegmatis*[42]). Finally, outlier SNPs for factor 4 included nonsynonymous mutations in *fas* (an essential gene involved in lipid metabolism with a potential role in antigenic recognition[43]) and *rpoC* (putatively associated with fitness cost compensation in rifampicin-resistant strains[44]).

We also sought to detect SNPs undergoing convergent evolution to identify possible beneficial mutations. We scrutinized an extended data set of 6,696 polymorphic sites with loosened thresholds of variant frequency and coverage to prevent the exclusion of positions below the thresholds for some genomes. Nevertheless, candidate SNPs still had to be covered by at least ten reads to be considered. Beyond known compensatory mutations in *rpoC*[45] and mutations in the promoter regions of drug resistance–associated genes (*eis*, *inhA* and *embA*), we identified 15 additional targets possibly under positive selection (**Supplementary Table 12**). Among these were nonsynonymous SNPs in *mmpL11* (putatively involved in fatty acid transport), *folC* (an essential gene involved in respiration) and *Rv2670c* (of unknown function), exclusively found in drug-resistant isolates in different monophyletic subgroups.

DISCUSSION

Using the largest data set of a single *M. tuberculosis* lineage ever investigated, we identified the population structure and reconstructed the evolutionary history of the Beijing lineage on a worldwide scale. The spatial distributions of strain haplotypes and allelic diversities, as well as the localization of ancestral CCs and branches, show that, in agreement with its historical designation, this lineage originated in the geographical zone centered on northeastern China, Korea and Japan. The time of its emergence, estimated at 6,600 years ago, is consistent with other recent data based on a much smaller strain collection[46] and is compatible with the onset of agriculture in that region[47]. Our data lead us to conclude that the worldwide spread of Beijing sublineages from this original focus occurred in several waves and was accompanied by important changes in the pathogen's population size, especially in the recent historical period, starting with industrialization and urbanization in the nineteenth century. The latest steps of this evolution include the specific epidemic expansion of two MDR clones throughout central Asia and Russia.

Our results suggest that, whereas the Asian sublineages (CC6 and BL7) arose during the late Neolithic, the two most recent clades appeared later (during the early medieval period) and gave rise to the European-Russian (CC2) and Pacific (CC5) branches. Interestingly, these two sublineages, as well as the central Asian (CC1) lineage, are also the ones showing the most recent traces of expansion, around 200 years ago, according to genotyping data. These recent expansions remarkably match known episodes of Chinese immigration. Major waves of Chinese settlement occurred on the Pacific Islands in the 1850s, along the navigation and trade routes across the Pacific Ocean and in North and South America, which might have promoted the

expansion of CC5 in this region[48]. Likewise, several waves of Chinese refugees migrated to the Russian empire, especially Kyrgyzstan, Kazakhstan and Uzbekistan, as a consequence of a series of national uprisings from 1861 to 1877, which might have driven the expansion of the CC1 and CC2 strains in these regions[49]. These recent western expansions are probably superimposed on a more historical, continuous flux of the different Beijing sublineages westward along the Silk Road.

Consistently, a sharp increase in the population size of the Beijing lineage as a whole was also detected concomitantly with the Industrial Revolution, around 200 years before the present, by Bayesian skyline analysis of genome-wide SNPs. The amount of SNP information available allowed us to detect even more recent changes in population size. The second abrupt surge in bacterial population size, detected around the period of the First World War, is fully in line with the documented peak in the tuberculosis death rate all over the globe due to the deprivations and comortality induced by the influenza pandemics at that time[50]. Our data additionally disclose the probable (but not necessarily exclusive) impact on the bacterial population of the large-scale onset of antibiotic use in the 1960s, which resulted in the first drop ever observed on the skyline plot, and of the HIV epidemics and/or increase in MDR populations, interrupting this fall.

Notably, our data indicate that the expansion of the two sublineages more frequently associated with MDR genotypes (central Asian (CC1) and European-Russian (CC2)) predated the era of antibiotics. This finding indicates that the prevalence of drug resistance in these CCs is not the primary cause of expansion but rather a consequence of public health–related and clinical weaknesses superimposed on a growing bacterial population. This hypothesis is supported by the specific, extremely low mean pairwise genetic distance of around 20 SNPs among the genomes of the MDR strain subsets of CC1 and CC2 (**Supplementary Fig. 10**). Assuming a mutation rate of 0.3–0.5 SNPs per genome per year[26,29,51], this finding indicates that the two corresponding original MDR clones started to spread epidemically only some 20–30 years ago across Eurasia, coinciding with the collapse of the public health system of the former Soviet Union. Of note, we found that a large clade (termed clade B), with limited genome-wide diversity among MDR strains from a local southwestern Russian population[3], is part of the same European-Russian W148 (CC2) outbreak defined in our global study (data not shown), which thus further demonstrates the epidemic spread of this clone.

Evidence for the higher virulence of modern Beijing strains in comparison with ancestral sublineage strains has been reported[52,53]. This difference might have contributed to the differential historical spread observed for these two sublineage groups (with, for example, the geographical restriction of CC6 and BL7).

We also detected an ensemble of gene variants potentially associated with the expansion of the modern Beijing strains by performing whole-genome scans for candidate SNPs and genes under positive selection unrelated to known targets of drug resistance. Among these, members of the *mce* and *vapBC* multigene families, associated with mycobacterial virulence[54] and the modulation of host immune response[55] and with growth control[56], respectively, appear as prominent candidates. Interestingly, we also identified sites within *Rv0176* (encoding an MCE1-associated protein) as being under diversifying selection by analyzing 73 genomes representing 6 of the 7 main MTBC lineages[57]. We also defined a list of other plausible gene targets under positive selection, associated with antibiotic resistance, fitness compensation, virulence and surface-exposed proteins, using a new Bayesian model-based SNP detection method. Of special interest is the identification of a frameshift mutation in the *kdpDE* operon, encoding a signal transduction system, which is a hallmark of the European-Russian W148 (CC2) sublineage. As a partial deletion of *kdpDE* in *M. tuberculosis* H37Rv has been shown to result in increased virulence in a mouse infection model[35], this frameshift mutation, putatively leading to a fusion protein of altered functionality, might well have contributed to the success of this clade. Hence, dismissing such phylogenetically informative SNPs as resulting from drift alone and not from selection might be misleading. This assumption is corroborated by an over-representation of genes associated with critical cell wall biosynthetic pathways among the functional families found for the other sublineage-specific SNPs detected by our Bayesian approach in comparison to those found for random SNPs ($P < 0.01$).

Finally, by screening for nucleotide positions under possible convergent evolution among drug-resistant isolates, we identified a set of new potential targets of drug resistance or fitness compensation mechanisms, including *mmpL11* and *Rv2670c*, in addition to expected genes such as *rpoC*, *embA*, *inhA* and *eis*. Our screen also captured *folC*, recently reported as a resistance-associated target by genome sequencing of 161 isolates from China[58]. Interestingly, polymorphisms in these genes are especially enriched in the European-Russian W148 (CC2) sublineage and are strongly associated with the MDR tuberculosis strains of MIRU-VNTR haplotype 100-32. Intriguingly, apart from expected genes and *folC*, we found virtually no overlap among the targets of positive selection associated with drug resistance identified in our study and in two other recent reports based on other strain samples and patient populations[58,59]. This lack of overlap suggests a potential influence from differences in strain genetic backgrounds, antituberculosis drug regimens and patient-dependent pharmacokinetics on the course and targets of selection.

In conclusion, our results show for the first time, to our knowledge, the important dynamic changes that have occurred in the worldwide population of a major *M. tuberculosis* lineage. Although the exact timing remains dependent upon uncertainties in mutation rates, especially over the long term, the conjunction of the most recent changes in the bacterial population with specific chief events in human history, as detected by using a molecular clock calibrated according to several convergent studies, is intriguing. Among other results, our analysis of European-Russian and central Asian sublineage demography illustrates how the effect of recent human interventions (the introduction of antibiotics followed by the development of multidrug resistance) has to be differentiated from pre-existing bacterial population changes to explain the regional prevalence of particular strains. Similar approaches could therefore be envisaged to better monitor and quantify the effects of future public health interventions (for example, new drugs and/or vaccines) on the pathogen population. From a more fundamental perspective, we propose that the expansion of modern Beijing strains has been favored by mutations in a number of gene targets under positive selection. The data obtained here thus suggest further experiments to investigate which of these candidate genes were involved. Such work may ultimately contribute to the detection of new targets for combating tuberculosis.

METHODS

Methods and any associated references are available in the online version of the paper.

Accession codes. Sequencing reads have been submitted to the EMBL-EBI European Nucleotide Archive (ENA) Sequence Read Archive (SRA) under the study accession PRJEB7281.

Note: Any Supplementary Information and Source Data files are available in the online version of the paper.

ACKNOWLEDGMENTS

We gratefully acknowledge L. Cowan and J. Posey (US Centers for Disease Control and Prevention) for providing us with significant amounts of genotyping data for *M. tuberculosis* Beijing isolates. We thank T. Ubben, I. Radzio, T. Struwe-Sonnenschein and J. Zallet (Research Center Borstel) for excellent technical assistance. We acknowledge J. Peh for her assistance and support in the study and I. Comas for statistical advice. Parts of this work have been supported by grants from the European Community's Seventh Framework Programme (FP7/2007-2013) under grant agreement 278864 in the framework of the European Union PathoNGenTrace project and grant agreement 223681 in the framework of the TB-PAN-NET project. We also thank Action Transversale du Muséum National d'Histoire Naturelle 'Les Microorganismes, Acteurs Clés dans les Ecosystèmes' for financial support. The funders had no role in study design, data collection and analysis, decision to publish or preparation of the manuscript.

AUTHOR CONTRIBUTIONS

I.M., P. Supply, S.N. and T.W. designed the study. M.M., P. Supply, S.N. and T.W. analyzed data and wrote the manuscript with comments from all authors. M.M., C.B., S. Mona and T.W. performed population genetics and phylogenetic analyses. M.M., N.D.-F., M. Blum and T.W. conducted selection tests. T.A.K. performed whole-genome sequencing and SNP calling. P. Supply, M.M., E.W., S.L., S.R.-G., I.M., S.N., E.A., C.A.-B., A.A., E.A.-K., M. Blum, F.B., H.P.B., C.E.B., M. Bonnet, E.B., I.C.-H., D.C., H.C., S.C., V.C., R.D., F.D., M.F.-D., S. Gagneux, S. Ghebremichael, M.H., S.H., W.-w.J., S.K., I.K., T.L., S. Maeda, V.N., M.R., N.R., S.S., E.S.-P., B.S., I.C.S., A.S., L.-H.S., P. Stakenas, K.T., F.V., D.V., C.W., M.B. and R.W. obtained mycobacterial genotyping data and drug susceptibility test results.

COMPETING FINANCIAL INTERESTS

The authors declare competing financial interests: details are available in the online version of the paper.

1. Global Tuberculosis Report. (World Health Organization, Geneva, 2013).
2. Klopper, M. *et al.* Emergence and spread of extensively and totally drug-resistant tuberculosis, South Africa. *Emerg. Infect. Dis.* **19**, 449–455 (2013).
3. Casali, N. *et al.* Evolution and transmission of drug-resistant tuberculosis in a Russian population. *Nat. Genet.* **46**, 279–286 (2014).
4. Stoffels, K. *et al.* From multidrug- to extensively drug-resistant tuberculosis: upward trends as seen from a 15-year nationwide study. *PLoS ONE* **8**, e63128 (2013).
5. Niemann, S. *et al. Mycobacterium tuberculosis* Beijing lineage favors the spread of multidrug-resistant tuberculosis in the Republic of Georgia. *J. Clin. Microbiol.* **48**, 3544–3550 (2010).
6. Mokrousov, I. Insights into the origin, emergence, and current spread of a successful Russian clone of *Mycobacterium tuberculosis*. *Clin. Microbiol. Rev.* **26**, 342–360 (2013).
7. Munsiff, S.S. *et al.* Persistence of a highly resistant strain of tuberculosis in New York City during 1990–1999. *J. Infect. Dis.* **188**, 356–363 (2003).
8. Cowley, D. *et al.* Recent and rapid emergence of W-Beijing strains of *Mycobacterium tuberculosis* in Cape Town, South Africa. *Clin. Infect. Dis.* **47**, 1252–1259 (2008).
9. Caminero, J.A. *et al.* Epidemiological evidence of the spread of a *Mycobacterium tuberculosis* strain of the Beijing genotype on Gran Canaria Island. *Am. J. Respir. Crit. Care Med.* **164**, 1165–1170 (2001).
10. Ford, C.B. *et al. Mycobacterium tuberculosis* mutation rate estimates from different lineages predict substantial differences in the emergence of drug-resistant tuberculosis. *Nat. Genet.* **45**, 784–790 (2013).
11. Comas, I. & Gagneux, S. A role for systems epidemiology in tuberculosis research. *Trends Microbiol.* **19**, 492–500 (2011).
12. Casali, N. *et al.* Microevolution of extensively drug-resistant tuberculosis in Russia. *Genome Res.* **22**, 735–745 (2012).
13. Glynn, J.R., Whiteley, J., Bifani, P.J., Kremer, K. & van Soolingen, D. Worldwide occurrence of Beijing/W strains of *Mycobacterium tuberculosis*: a systematic review. *Emerg. Infect. Dis.* **8**, 843–849 (2002).
14. Bifani, P.J., Mathema, B., Kurepina, N.E. & Kreiswirth, B.N. Global dissemination of the *Mycobacterium tuberculosis* W-Beijing family strains. *Trends Microbiol.* **10**, 45–52 (2002).
15. Parwati, I., van Crevel, R. & van Soolingen, D. Possible underlying mechanisms for successful emergence of the *Mycobacterium tuberculosis* Beijing genotype strains. *Lancet Infect. Dis.* **10**, 103–111 (2010).
16. Hanekom, M. *et al. Mycobacterium tuberculosis* Beijing genotype: a template for success. *Tuberculosis (Edinb.)* **91**, 510–523 (2011).
17. de Jong, B.C. *et al.* Progression to active tuberculosis, but not transmission, varies by *Mycobacterium tuberculosis* lineage in The Gambia. *J. Infect. Dis.* **198**, 1037–1043 (2008).
18. Kato-Maeda, M. *et al.* Beijing sublineages of *Mycobacterium tuberculosis* differ in pathogenicity in the guinea pig. *Clin. Vaccine Immunol.* **19**, 1227–1237 (2012).
19. Weniger, T., Krawczyk, J., Supply, P., Niemann, S. & Harmsen, D. MIRU-VNTRplus: a web tool for polyphasic genotyping of *Mycobacterium tuberculosis* complex bacteria. *Nucleic Acids Res.* **38**, W326–W331 (2010).
20. Plikaytis, B.B. *et al.* Multiplex PCR assay specific for the multidrug-resistant strain W of *Mycobacterium tuberculosis*. *J. Clin. Microbiol.* **32**, 1542–1546 (1994).
21. Kalinowski, S.T. Counting alleles with rarefaction: private alleles and hierarchicalsampling design. *Conserv. Genet.* **5**, 539–543 (2004).
22. Supply, P., Niemann, S. & Wirth, T. On the mutation rates of spoligotypes and variable numbers of tandem repeat loci of *Mycobacterium tuberculosis*. *Infect. Genet. Evol.* **11**, 251–252 (2011).
23. Reyes, J.F. & Tanaka, M.M. Mutation rates of spoligotypes and variable numbers of tandem repeat loci in *Mycobacterium tuberculosis*. *Infect. Genet. Evol.* **10**, 1046–1051 (2010).
24. Ragheb, M.N. *et al.* The mutation rate of mycobacterial repetitive unit loci in strains of *M. tuberculosis* from cynomolgus macaque infection. *BMC Genomics* **14**, 145 (2013).
25. Comas, I., Homolka, S., Niemann, S. & Gagneux, S. Genotyping of genetically monomorphic bacteria: DNA sequencing in mycobacterium tuberculosis highlights the limitations of current methodologies. *PLoS ONE* **4**, e7815 (2009).
26. Walker, T.M. *et al.* Whole-genome sequencing to delineate *Mycobacterium tuberculosis* outbreaks: a retrospective observational study. *Lancet Infect. Dis.* **13**, 137–146 (2013).
27. Nieselt-Struwe, K. & von Haeseler, A. Quartet-mapping, a generalization of the likelihood-mapping procedure. *Mol. Biol. Evol.* **18**, 1204–1219 (2001).
28. Namouchi, A., Didelot, X., Schock, U., Gicquel, B. & Rocha, E.P. After the bottleneck: genome-wide diversification of the *Mycobacterium tuberculosis* complex by mutation, recombination, and natural selection. *Genome Res.* **22**, 721–734 (2012).
29. Roetzer, A. *et al.* Whole genome sequencing versus traditional genotyping for investigation of a *Mycobacterium tuberculosis* outbreak: a longitudinal molecular epidemiological study. *PLoS Med.* **10**, e1001387 (2013).
30. Ford, C.B. *et al.* Use of whole genome sequencing to estimate the mutation rate of *Mycobacterium tuberculosis* during latent infection. *Nat. Genet.* **43**, 482–486 (2011).
31. Comas, I. & Gagneux, S. The past and future of tuberculosis research. *PLoS Pathog.* **5**, e1000600 (2009).
32. Colditz, G.A. *et al.* Efficacy of BCG vaccine in the prevention of tuberculosis. Meta-analysis of the published literature. *J. Am. Med. Assoc.* **271**, 698–702 (1994).
33. Holden, C. Stalking a killer in Russia's prisons. *Science* **286**, 1670 (1999).
34. Bifani, P.J. *et al.* Origin and interstate spread of a New York City multidrug-resistant *Mycobacterium tuberculosis* clone family. *J. Am. Med. Assoc.* **275**, 452–457 (1996).
35. Parish, T. *et al.* Deletion of two-component regulatory systems increases the virulence of *Mycobacterium tuberculosis*. *Infect. Immun.* **71**, 1134–1140 (2003).
36. Duforet-Frebourg, N., Bazin, E. & Blum, M.G. Genome scans for detecting footprints of local adaptation using a Bayesian factor model. *Mol. Biol. Evol.* **31**, 2483–2495 (2014).
37. Maloney, E. *et al.* The two-domain LysX protein of *Mycobacterium tuberculosis* is required for production of lysinylated phosphatidylglycerol and resistance to cationic antimicrobial peptides. *PLoS Pathog.* **5**, e1000534 (2009).
38. Sirakova, T.D., Fitzmaurice, A.M. & Kolattukudy, P. Regulation of expression of *mas* and *fadD28*, two genes involved in production of dimycocerosyl phthiocerol, a virulence factor of *Mycobacterium tuberculosis*. *J. Bacteriol.* **184**, 6796–6802 (2002).
39. Ebrahimi-Rad, M. *et al.* Mutations in putative mutator genes of *Mycobacterium tuberculosis* strains of the W-Beijing family. *Emerg. Infect. Dis.* **9**, 838–845 (2003).
40. Etienne, G. *et al.* Identification of the polyketide synthase involved in the biosynthesis of the surface-exposed lipooligosaccharides in mycobacteria. *J. Bacteriol.* **191**, 2613–2621 (2009).
41. Ahmad, S., El-Shazly, S., Mustafa, A.S. & Al-Attiyah, R. Mammalian cell-entry proteins encoded by the *mce3* operon of *Mycobacterium tuberculosis* are expressed during natural infection in humans. *Scand. J. Immunol.* **60**, 382–391 (2004).
42. Li, X.Z., Zhang, L. & Nikaido, H. Efflux pump–mediated intrinsic drug resistance in *Mycobacterium smegmatis*. *Antimicrob. Agents Chemother.* **48**, 2415–2423 (2004).
43. Meikle, V. *et al.* Identification of novel *Mycobacterium bovis* antigens by dissection of crude protein fractions. *Clin. Vaccine Immunol.* **16**, 1352–1359 (2009).
44. de Vos, M. *et al.* Putative compensatory mutations in the *rpoC* gene of rifampin-resistant *Mycobacterium tuberculosis* are associated with ongoing transmission. *Antimicrob. Agents Chemother.* **57**, 827–832 (2013).
45. Comas, I. *et al.* Whole-genome sequencing of rifampicin-resistant *Mycobacterium tuberculosis* strains identifies compensatory mutations in RNA polymerase genes. *Nat. Genet.* **44**, 106–110 (2012).
46. Comas, I. *et al.* Out-of-Africa migration and Neolithic coexpansion of *Mycobacterium tuberculosis* with modern humans. *Nat. Genet.* **45**, 1176–1182 (2013).
47. Fuller, D.Q. *et al.* The domestication process and domestication rate in rice: spikelet bases from the Lower Yangtze. *Science* **323**, 1607–1610 (2009).
48. Fang, J. *Atlas for Sustainability in Polynesian Island Cultures and Ecosystems* (Sea Education Association, 2013).

49. Laruelle, M. & Peyrouse, S. Cross-border minorities as cultural and economic mediators between China and Central Asia. *China and Eurasia Forum Quarterly* **7**, 93–119 (2009).
50. Drolet, G.J. World War I and tuberculosis. A statistical summary and review. *Am. J. Public Health Nations Health* **35**, 689–697 (1945).
51. Bryant, J.M. *et al.* Inferring patient to patient transmission of *Mycobacterium tuberculosis* from whole genome sequencing data. *BMC Infect. Dis.* **13**, 110 (2013).
52. Aguilar, D. *et al. Mycobacterium tuberculosis* strains with the Beijing genotype demonstrate variability in virulence associated with transmission. *Tuberculosis (Edinb.)* **90**, 319–325 (2010).
53. Ribeiro, S.C. *et al. Mycobacterium tuberculosis* strains of the modern sublineage of the Beijing family are more likely to display increased virulence than strains of the ancient sublineage. *J. Clin. Microbiol.* **52**, 2615–2624 (2014).
54. Gioffré, A. *et al.* Mutation in *mce* operons attenuates *Mycobacterium tuberculosis* virulence. *Microbes Infect.* **7**, 325–334 (2005).
55. Stavrum, R. *et al.* Modulation of transcriptional and inflammatory responses in murine macrophages by the *Mycobacterium tuberculosis* mammalian cell entry (Mce) 1 complex. *PLoS ONE* **6**, e26295 (2011).
56. Ahidjo, B.A. *et al.* VapC toxins from *Mycobacterium tuberculosis* are ribonucleases that differentially inhibit growth and are neutralized by cognate VapB antitoxins. *PLoS ONE* **6**, e21738 (2011).
57. Osório, N.S. *et al.* Evidence for diversifying selection in a set of *Mycobacterium tuberculosis* genes in response to antibiotic- and nonantibiotic-related pressure. *Mol. Biol. Evol.* **30**, 1326–1336 (2013).
58. Zhang, H. *et al.* Genome sequencing of 161 *Mycobacterium tuberculosis* isolates from China identifies genes and intergenic regions associated with drug resistance. *Nat. Genet.* **45**, 1255–1260 (2013).
59. Farhat, M.R. *et al.* Genomic analysis identifies targets of convergent positive selection in drug-resistant *Mycobacterium tuberculosis*. *Nat. Genet.* **45**, 1183–1189 (2013).

[1]Molecular Mycobacteriology, Research Center Borstel, Borstel, Germany. [2]Laboratoire Biologie Intégrative des Population, Evolution Moléculaire, Ecole Pratique des Hautes Etudes, Paris, France. [3]Muséum National d'Histoire Naturelle, l'Institut de Systématique, Évolution, Biodiversité, UMR–Centre National de la Recherche Scientifique 7205, Département Systématique et Evolution, Paris, France. [4]Université Joseph Fourier, Centre National de la Recherche Scientifique, Laboratoire Techniques de l'Ingénierie Médicale et de la Complexité–Informatique, Mathématiques et Applications, Grenoble, France. [5]INSERM U1019, Center for Infection and Immunity of Lille, Lille, France. [6]Centre National de la Recherche Scientifique, UMR 8204, Lille, France. [7]Université Lille Nord, Center for Infection and Immunity of Lille, Lille, France. [8]Institut Pasteur de Lille, Center for Infection and Immunity of Lille, Lille, France. [9]National Reference Center for Mycobacteria, Research Center Borstel, Borstel, Germany. [10]Laboratory of Molecular Microbiology, St. Petersburg Pasteur Institute, St. Petersburg, Russia. [11]Centre for Biomedical Research, Burnet Institute, Melbourne, Victoria, Australia. [12]Genoscreen, Lille, France. [13]Medical Department, Médecins sans Frontières Switzerland, Geneva, Switzerland. [14]Department of Microbiology, National Tuberculosis and Lung Diseases Research Institute, Warsaw, Poland. [15]Institute of Social and Preventive Medicine, University of Bern, Bern, Switzerland. [16]Instituto de Medicina Tropical Alexander von Humboldt, Molecular Epidemiology Unit–Tuberculosis, Universidad Peruana Cayetano Heredia, Lima, Peru. [17]Department of Medical Parasitology and Infection Biology, Swiss Tropical and Public Health Institute, Basel, Switzerland. [18]Tuberculosis Research Section, National Institute of Allergy and Infectious Diseases, US National Institutes of Health, Bethesda, Maryland, USA. [19]Clinical Research Department, Epicentre, Paris, France. [20]Emerging Bacterial Pathogens Unit, San Raffaele Scientific Institute, Milan, Italy. [21]Department of Microbiology, Hospital Universitario de Gran Canaria Dr. Negrín, Las Palmas de Gran Canaria, Spain. [22]Division of Medical Microbiology, University of Cape Town, Cape Town, South Africa. [23]Department of Infectious Diseases, Alfred Hospital, Melbourne, Victoria, Australia. [24]Central Clinical School, Monash University, Melbourne, Victoria, Australia. [25]National Tuberculosis Reference Laboratory, Phthysiopneumology Institute, Chisinau, Republic of Moldova. [26]Institute for Epidemiology, Schleswig-Holstein University Hospital, Kiel, Germany. [27]Public Health England National Mycobacterial Reference Laboratory and Clinical Tuberculosis and Human Immunodeficiency Virus Group, Queen Mary's School of Medicine and Dentistry, London, UK. [28]Department of Infectious Diseases, Imperial College, London, UK. [29]Tuberculosis and Mycobacteria, Scientific Institute of Public Health, Brussels, Belgium. [30]Department of Microbiology, Public Health Agency of Sweden, Solna, Sweden. [31]Department of Science and Technology/National Research Foundation, Centre of Excellence for Biomedical Tuberculosis Research/Medical Research Council, Centre for Tuberculosis Research, Division of Molecular Biology and Human Genetics, Faculty of Medicine and Health Sciences, Stellenbosch University, Cape Town, South Africa. [32]Department of Diagnostics and Vaccinology, Swedish Institute for Communicable Disease Control, Solna, Sweden. [33]Key Laboratory of Major Diseases in Children and National Key Discipline of Pediatrics (Capital Medical University), Ministry of Education, Beijing Pediatric Research Institute, Beijing Children's Hospital, Capital Medical University, Beijing, China. [34]US Agency for International Development Quality Health Care Project, Bishkek, Kyrgyzstan. [35]Samara Oblast Tuberculosis Service, Samara, Russia. [36]Statens Serum Institute, International Reference Laboratory of Mycobacteriology, Copenhagen, Denmark. [37]Research Institute of Tuberculosis, Japan Anti-Tuberculosis Association, Tokyo, Japan. [38]World Health Organization Supranational Tuberculosis Reference Laboratory, Institut Pasteur de la Guadeloupe, Abymes, France. [39]Instituto de Investigación Sanitaria Aragón, Hospital Universitario Miguel Servet, Zaragoza, Spain. [40]Institute of Microbiology and Immunology, Faculty of Medicine, University of Belgrade, Belgrade, Serbia. [41]Central Tuberculosis Laboratory, Department of Pathology, Singapore General Hospital, Singapore. [42]Department of Immunology and Cell Biology, Institute of Biotechnology, Vilnius University, Vilnius, Lithuania. [43]Tartu University Hospital United Laboratories, Mycobacteriology, Tartu, Estonia. [44]Medical Department, Médecins sans Frontières, Paris, France. [45]German Center for Infection Research, Borstel Site, Borstel, Germany. [46]These authors contributed equally to this work. Correspondence should be addressed to T.W. (wirth@mnhn.fr), P. Supply (philip.supply@ibl.cnrs.fr) or S.N. (sniemann@fz-borstel.de).

ONLINE METHODS

Sampling and data collection. The study is based on a global collection of clinical isolates of *M. tuberculosis* Beijing (**Supplementary Tables 1** and **2**). The data set contains the 24-locus MIRU-VNTR genotypes for 4,987 strains from 99 countries (**Supplementary Fig. 1**). *M. tuberculosis* isolates were genotyped by multiplex PCR amplification as described previously[60,61]. Amplicons were subjected to electrophoretic analysis using ABI 3100 and 3730 automated sequencers. Sizing of the PCR fragments and assignment of VNTR alleles at the 24 loci were performed using GENEMAPPER software (PE Applied Biosystems).

MIRU data analyses. *Genetic diversity estimation and population structure.* The number of alleles (allelic richness) in each *M. tuberculosis* clonal group or biologically relevant population was estimated, and sample sizes were corrected by the rarefaction procedure using HP-RARE[62]. Comparison tests as well as *P* values were estimated using the STATISTICA v.6.1 package.

The population structure based on 24-locus MIRU-VNTR data for 4,987 clinical *M. tuberculosis* Beijing isolates was inferred with the minimum spanning tree (MSTREE) algorithm implemented in BioNumerics software package v6.7 (Applied Maths). Strains with an identical MIRU-VNTR haplotype were pooled in a single node in the MSTREE and thereby represent a cluster. The rate of clustered strains was considered as an indicator for the extent of recent transmission among the Beijing sublineages.

Biogeography. We evaluated the allelic richness of each geographical sample where 24-locus MIRU-VNTR haplotypes were available for at least 23 isolates using the software HP-RARE[21]. This software computes a rarefaction to avoid the bias created by differences in sampling size. We then computed the geographical distances (shortest walking distance according to classic human migration routes) between all 40 corresponding geographical locations and the Yangtze delta region using tools implemented in Google Earth. This step was followed by the calculation of a linear correlation (r^2) between the allelic richness of an area and the geographical distance from the source. For the geographical mapping of Beijing clonal complexes on the world map, we used MLVA Compare v1.03 (Ridom) and the implemented geocoding option.

Coalescence, TMRCA and demography. In a first step, we used a Bayesian-based coalescent approach[63] on MIRU-VNTR data. It assumes a stepwise mutation model of MIRU evolution, and it estimates the posterior probability distributions of the genealogical and demographic parameters of a sample using Markov chain Monte Carlo (MCMC) simulations. This method permits inferences of important biological parameters such as the TMRCA of a given sample, the past and present effective population sizes, and the latest demographic changes (decline, constant population size or expansion). Given the absence of recombination (as confirmed by whole-genome sequence analysis), we inferred demographic parameters from the 24-locus data under a Bayesian-based coalescent approach implemented in the software BATWING for linked tandem repeat loci[64,65]. The coalescent prior used for the distribution of topology and branch lengths of the gene genealogy was a three-parameter model: a constant ancestral population size experiencing an exponential population expansion at some time in the past[64]. The likelihood of the gene genealogy was computed under the stepwise mutation model[66]. The posterior probabilities of the gene genealogy, population genetics parameters and MIRU-VNTR mutation rates were approximated through the Metropolis-Hastings algorithm[67,68]. Time of population expansion and modern effective population size were scaled relative to the ancestral population size under the model implemented in BATWING. To test for prior sensitivity and to check for convergence, we ran all the analyses using two different priors for the ancestral population size: we tested both a normal distribution N (5×10^7; 1×10^7) and a uniform distribution U (1×10^3; 1×10^8). The results were consistent between the runs, and we present only the results obtained under the normal prior. We therefore placed an independent uniform prior for the mutation rate of each MIRU-VNTR locus, bounded between 9×10^{-8} and 9×10^{-7} per locus per generation, according to previous studies[69]. All the analyses were run for 1 billion MCMC generations, using a thinning interval of 100,000. The MCMC output was analyzed using the library coda available under the R environment (R Development Core Team 2011) to obtain the posterior distribution and the effective sample size (ESS) of all parameters (which were all above 150).

Genome data analyses. *Strain selection for whole-genome sequencing analysis.* For whole-genome sequencing and phylogenetic reconstruction, strains were selected according to two priority rules: first, to represent major nodes in our MIRU-VNTR–based minimum spanning tree and their main adjacent multi-locus variants and, second, to cover different countries of origin and/or different studies. As a result, the proportions of isolates from the 7 identified complexes were in a similar range, i.e., 29/907 (3.2%) for CC1, 19/457 (4.2%) for CC2, 14/972 (1.4%) for CC3, 18/1,027 (1.8%) for CC4, 11/542 (2.0%) for CC5, 7/475 (1.5%) for CC6 and 12/607 (2.0%) for BL7. CC1 and CC2 were somewhat over-represented to better confirm the outbreak-related nature of isolates subsequently termed as central Asian and European-Russian W148 outbreaks, respectively, and with a comparable very low mean pairwise genetic distance of around 20 SNPs. Again, this selection was carried out by considering isolates from different regions and studies (**Supplementary Table 3**).

Variant detection. Whole-genome sequencing was performed with Illumina technology (MiSeq) using Nextera XT library preparation kits as instructed by the manufacturer (Illumina). Raw data (fastq files) were submitted to the EMBL-EBI ENA SRA under the study accession PRJEB7281. Resulting reads were mapped to the *M. tuberculosis* H37Rv genome sequence (GenBank, NC_000962.3) using the exact alignment program SARUMAN[70]. High-quality SNPs with a minimum of 10× coverage and 75% variant frequency were extracted and combined for all analyzed isolates ($n = 110$) using customized Perl scripts. We used only genome positions with high-quality variant calls for every isolate (that met the thresholds for coverage and variant frequency) for a concatenated sequence alignment. For phylogenetic inference, we excluded drug resistance–associated genes, repetitive regions and artifactual variant calls resulting from indels in single strains.

Likelihood mapping. The phylogenetic signal of the data set was investigated with the likelihood mapping method implemented in TREE-PUZZLE[71] by analyzing 10,000 random quartets. This method proceeds by evaluating, using maximum-likelihood, groups of four randomly chosen sequences (quartets). The three possible unrooted tree topologies for each quartet are weighted, and the posterior weights are then plotted using triangular coordinates, such that each corner represents a fully resolved tree topology. Therefore, the resulting distribution of the points shows whether the data are suitable for a phylogenetic reconstruction.

Recombination detection. Most of the analyses developed in our analytical framework (phylogenetics and Bayesian inference) are based on the assumption that *M. tuberculosis* evolution is mostly clonal and that recombination can be neglected. Therefore, in a preliminary step, we tested the presence of mosaic genomes or possible HGT with the algorithm SPLITSTREE. Each data set was analyzed for the presence of recombinant sequences using the PHI test with $\alpha = 0.001$.

Phylogenetic inferences. Phylogenetic relationships were reconstructed using the maximum-likelihood approach implemented in PHYML 3.412 (ref. 72). The robustness of the maximum-likelihood tree topology was assessed with bootstrapping analyses of 1,000 pseudoreplicated data sets. A transversion substitution model (TVM) was selected on the basis of Akaike's information criterion using JMODELTEST[73]. Phylogenies were rooted with the midpoint rooting option using FigTree software v1.4 and with the reference *M. tuberculosis* strain H37Rv, both resulting in the same topology.

Coalescent-based analyses. Evolutionary rates and tree topologies were analyzed using the general time-reversible (GTR) and Hasegawa-Kishino-Yano[74] (HKY) substitution models with gamma distributed among-site rate variation with four rate categories (Γ4). We tested both a strict molecular clock (which assumes the same evolutionary rates for all branches in the tree) and a relaxed clock that allows different rates among branches. Constant-sized, logistic, exponentially growing coalescent models were used. We also considered the Bayesian skyline plot model[75], based on a general, non-parametric prior that enforces no particular demographic history. We used a piecewise linear skyline model with ten groups, and we then compared the marginal likelihood for each model using Bayes factors estimated in TRACER 1.5. Bayes factors represent the ratio of the marginal likelihood of the models being compared. Approximate marginal likelihoods for each coalescent model were calculated via importance sampling (1,000 bootstraps) using the harmonic mean of the sampled likelihoods. A ratio between 3 and 10 indicates moderate support that one model better fits the data than another, whereas values greater than 10 indicate strong support.

For each analysis, 2 independent runs of 100 million steps were performed, and the chain was sampled every 10,000 generations. Examination of the MCMC samples with TRACER 1.5 indicated convergence and adequate mixing of the Markov chains, with ESSs for each parameter in the hundreds or thousands. The first 10% of each chain were discarded as burn-in. We found the maximum clade credibility topology using TREEANNOTATOR 1.7.5 (ref. 76), and we reconstructed the Bayesian skyline plot using TRACER 1.5. The relaxed clock models provided better fit to the data (Bayes factor > 12); under the different models tested, the Bayesian skyline model provided the better fit overall (marginally better).

Analysis of genes under positive selection. We selected all genes that are associated with the four *M. tuberculosis mce* operons[77] and known T cell antigens[45]. Polymerases and ribosomal proteins as well as *vapBC* and *fad* genes were selected from a free text search under http://tuberculist.epfl.ch/ using the terms "polymerase," "vap" and "fad". All genes with an annotated function of "lipoprotein" from the H37Rv reference genome (GenBank, NC_000962.3) were selected. Furthermore, we selected 300 essential and 300 non-essential genes by assigning random numbers with the MS Excel function = RAND () to all H37Rv genes and choosing the top 300 largest numbers in the respective category.

For the dN/dS analysis, we prepared concatenated gene sequences for all MRCAs of modern Beijing subgroups and compared them pairwise with the MRCA of the entire Beijing lineage. Ancestral states were inferred from the maximum likelihood–based phylogeny. The dN/dS ratio was calculated using the software KaKs calculator (v1.2)[78] with the Nei-Gojobori method. It was not possible to calculate a dN/dS ratio for all subgroups because of the absence of either nonsynonymous or synonymous SNPs. Furthermore, we counted the number of nonsynonymous and synonymous SNPs unique to all modern or ancestral subgroups and used a χ^2 test with Yates correction to compare amino acid changes affecting analyzed gene families to the random selection of essential and non-essential genes, respectively. Pairwise tests were carried out with modern Beijing subgroup SNPs and with ancestral Beijing subgroup SNPs separately. Homoplastic and convergent SNPs were identified via visual examination of the distribution of an extended set of 6,696 concatenated polymorphic sites across different Beijing subgroups.

Additionally, to capture SNPs under positive selection, we applied the software PCADAPT to perform a genome scan based on a Bayesian factor model[36]. We chose $K = 4$ factors because the fifth and the sixth factors did not correspond to population structure and distinguished individuals within the same clades. The factor analysis was performed on the centered genotype matrix that was not scaled. The MCMC algorithm was initialized using singular value decomposition, and the total number of steps was equal to 400 with a burn-in of 200 steps.

60. Supply, P. *et al.* Automated high-throughput genotyping for study of global epidemiology of *Mycobacterium tuberculosis* based on mycobacterial interspersed repetitive units. *J. Clin. Microbiol.* **39**, 3563–3571 (2001).
61. Supply, P. *et al.* Proposal for standardization of optimized mycobacterial interspersed repetitive unit–variable number tandem repeat typing of *Mycobacterium tuberculosis*. *J. Clin. Microbiol.* **44**, 4498–4510 (2006).
62. Kalinowski, S.T. HP-rare: a computer program for performing rarefaction on measures of allelic diversity. *Mol. Ecol. Notes* **5**, 187–189 (2005).
63. Beaumont, M.A. Detecting population expansion and decline using microsatellites. *Genetics* **153**, 2013–2029 (1999).
64. Wilson, I.J., Weale, M.E. & Balding, D.J. Inferences from DNA data: population histories, evolutionary processes and forensic match probabilities. *J. R. Stat. Soc. Ser. A Stat. Soc.* **166**, 155–188 (2003).
65. Wilson, I.J. & Balding, D.J. Genealogical inference from microsatellite data. *Genetics* **150**, 499–510 (1998).
66. Ohta, T. & Kimura, M. A model of mutation appropriate to estimate the number of electrophoretically detectable alleles in a finite population. *Genet. Res.* **22**, 201–204 (1973).
67. Metropolis, N., Rosenbluth, A.W., Rosenbluth, M.N., Teller, A.H. & Teller, E. Equations of state calculations by fast computing machine. *J. Chem. Phys.* **21**, 1087–1091 (1953).
68. Hastings, W.K. Monte Carlo sampling methods using Markov chains and their applications. *Biometrika* **57**, 97–109 (1970).
69. Wirth, T. *et al.* Origin, spread and demography of the *Mycobacterium tuberculosis* complex. *PLoS Pathog.* **4**, e1000160 (2008).
70. Blom, J. *et al.* Exact and complete short-read alignment to microbial genomes using Graphics Processing Unit programming. *Bioinformatics* **27**, 1351–1358 (2011).
71. Schmidt, H.A., Strimmer, K., Vingron, M. & von Haeseler, A. TREE-PUZZLE: maximum likelihood phylogenetic analysis using quartets and parallel computing. *Bioinformatics* **18**, 502–504 (2002).
72. Guindon, S. & Gascuel, O. A simple, fast, and accurate algorithm to estimate large phylogenies by maximum likelihood. *Syst. Biol.* **52**, 696–704 (2003).
73. Posada, D. & Crandall, K.A. MODELTEST: testing the model of DNA substitution. *Bioinformatics* **14**, 817–818 (1998).
74. Hasegawa, M., Kishino, H. & Yano, T. Dating of the human-ape splitting by a molecular clock of mitochondrial DNA. *J. Mol. Evol.* **22**, 160–174 (1985).
75. Drummond, A.J., Rambaut, A., Shapiro, B. & Pybus, O.G. Bayesian coalescent inference of past population dynamics from molecular sequences. *Mol. Biol. Evol.* **22**, 1185–1192 (2005).
76. Drummond, A.J. & Rambaut, A. BEAST: Bayesian evolutionary analysis by sampling trees. *BMC Evol. Biol.* **7**, 214 (2007).
77. Casali, N. & Riley, L.W. A phylogenomic analysis of the Actinomycetales *mce* operons. *BMC Genomics* **8**, 60 (2007).
78. Zhang, Z. *et al.* KaKs_Calculator: calculating Ka and Ks through model selection and model averaging. *Genomics Proteomics Bioinformatics* **4**, 259–263 (2006).

AAC
Journals.ASM.org

Association between *pncA* Gene Mutations, Pyrazinamidase Activity, and Pyrazinamide Susceptibility Testing in *Mycobacterium tuberculosis*

Akio Aono,[a] Kinuyo Chikamatsu,[a] Hiroyuki Yamada,[a] Tomoko Kato,[a,b] Satoshi Mitarai[a,b]

Department of Mycobacterium Reference and Research, The Research Institute of Tuberculosis, Japan Anti-Tuberculosis Association, Kiyose, Japan[a]; Basic Mycobacteriosis, Nagasaki University Graduate School of Biomedical Sciences, Nagasaki, Japan[b]

We determined MICs for, confirmed the presence of *pncA* mutations in, and performed pyrazinamidase testing on colonies (subclones) obtained from seven isolates that exhibited differential pyrazinamide (PZA) susceptibility. Six of the seven strains were found to exhibit characteristics resulting from the mixture of strains possessing different properties. In addition, our analysis revealed large *pncA*-spanning deletions (1,565 bp, 4,475 bp, and 6,258 bp) in three strains that showed high PZA resistance.

Pyrazinamide (PZA) is an important drug used in the treatment of tuberculosis (1). The conversion of PZA to pyrazinoic acid (POA) by pyrazinamidase (PZase) is necessary for its activity. Bacterial resistance to PZA has been shown to correlate with mutations in the *pncA* gene that encodes PZase (2, 3, 4).

The antimicrobial activity of PZA is considerably affected by the pH of its environment (5). The Bactec MGIT 960 system (Becton, Dickinson, Sparks, MD) was used to measure PZA drug susceptibility (6, 7) in bacteria grown in liquid medium that was adjusted to pH 5.9 (8). However, the MGIT system has generated inconsistent test outcomes when assessing PZase activity and the presence of *pncA* mutations (9, 10, 11).

In this study, we evaluated PZA drug susceptibility in 83 multidrug-resistant *Mycobacterium tuberculosis* strains (recently isolated in Japan) by using MGIT and PZase testing, and we confirmed the presence of *pncA* mutations in these strains. The strains were examined for their susceptibility to 100 μg/ml of PZA by using an MGIT PZA antimicrobial susceptibility testing assay, as previously described (8). For the strains that demonstrated resistance to 100 μg/ml PZA, the PZA MIC was determined using the EpiCenter system (Becton, Dickinson) by dissolving PZA powder to 200, 300, 400, 800, and 1,600 μg/ml in MGIT culture medium. PZase analysis was conducted using Wayne's method (12).

Using PCR, *pncA* was amplified from each strain and then directly sequenced according to the methods described by Sreevatsan et al. (13). The 673-bp region spanning *pncA* and an 82-bp upstream sequence amplified using *pncA* primers (see Table S1 in the supplemental material) were purified using MagExtractor (Toyobo, Osaka, Japan). The PCR products were then directly sequenced using a BigDye Terminator v3.1 cycle sequencing kit (Applied Biosystems) and an ABI 3137 sequencer (Applied Biosystems). The *pncA* sequences were compared to the H37Rv strain genome (ATCC 27294) by using Genetyx Win v5.2 (Genetyx Co., Japan). In cases where PCR failed to yield a *pncA* amplicon, the strains were probed for amplification products upstream and downstream of *pncA* to investigate the cause of the negative results. PCR products were directly sequenced using the primer sets that were used for amplification.

The strains that differed with respect to *pncA* mutation or PZase activity at an MIC of ≥200 μg/ml and that were resistant to PZA were subcultured, and 10 subclones were randomly selected for each strain. Each subclone was again subjected to MIC and PZase testing and *pncA* mutation confirmation. The subclones were compared using a 15-locus variable-number tandem repeat (VNTR) analysis, as described by Supply et al. (14).

Three of the 83 strains were excluded from the study because of contamination. Of the remaining 80 strains, 31 (38.8%) showed susceptibility in the MGIT PZA assay, carried no *pncA* mutations, and tested positive for PZase, whereas 49 strains (61.2%) showed a PZA MIC of ≥200 μg/ml. Of these 49 strains, 39 (79.6%) carried a *pncA* mutation and were PZase negative (Fig. 1; see also Table S2 in the supplemental material). Colonies from 7 of the 49 strains (14.3%) which differed with respect to *pncA* mutation or PZase activity and exhibited a PZA MIC of ≥200 μg/ml were subcultured. Each subclone was again subjected to MIC and PZase testing and to *pncA* mutation confirmation (Table 1). Strain 4 displayed characteristics from two different subclones: (i) had a PZA MIC of ≤100 μg/ml, carried no *pncA* mutation, and was PZase positive, and (ii) had a PZA MIC of 1,600 μg/ml, carried a *pncA* mutation, and was PZase negative. Strains 13, 17, 50, and 79 displayed the following subclone characteristics: (i) had a PZA MIC of ≤100 μg/ml, and (ii) had a PZA MIC of ≥200 μg/ml, carried no *pncA* mutation, and were PZase positive. Strain 25 exhibited characteristics of three subclones: (i) had a PZA MIC of ≤100 μg/ml, carried no *pncA* mutation, and was PZase positive, (ii) had a PZA MIC of 400 μg/ml, carried no *pncA* mutation, and was PZase positive, and (iii) had a PZA MIC of ≥1,600 μg/ml, carried no *pncA* mutation, and was PZase negative. Strain 6 had an MIC of ≤100 μg/ml, showed no *pncA* mutation, and was PZase positive. No strain exhibiting an MIC of ≥200 μg/ml was isolated. VNTR analysis was conducted to compare the subclones from the six strains that exhibited mixed-strain characteristics. We found that the copy numbers were identical in each strain for each locus except for strain 17, which had a difference on QUB11b.

These results indicated that six of the seven strains exhibited

Received 28 January 2014 Returned for modification 4 March 2014
Accepted 18 May 2014
Published ahead of print 27 May 2014
Address correspondence to Akio Aono, aono@jata.or.jp.
Supplemental material for this article may be found at http://dx.doi.org/10.1128/AAC.02394-14.

doi:10.1128/AAC.02394-14

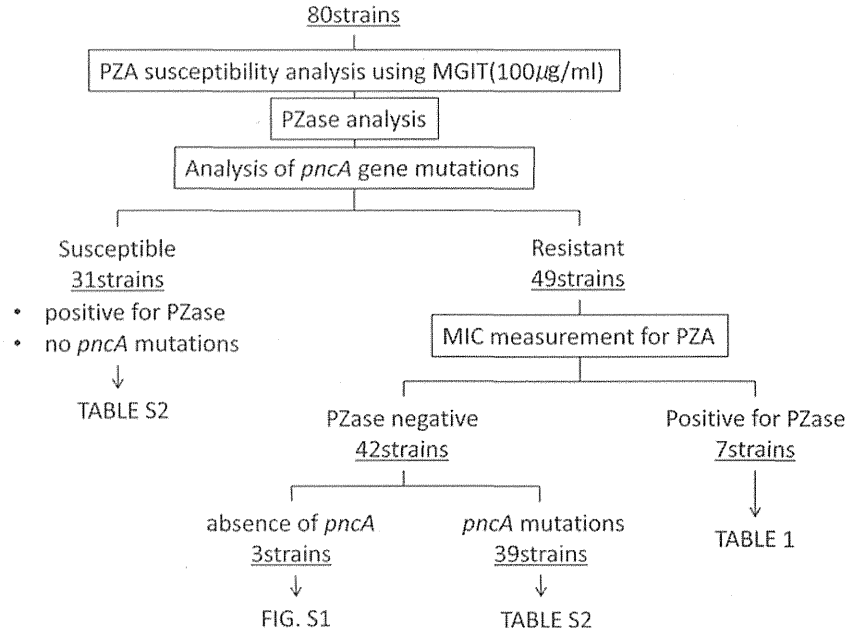

FIG 1 Flow diagram of PZA susceptibility analysis, *pncA* mutation testing, PZase analysis, and PZA MIC determinations (see also Fig. S1 and Table S2 in the supplemental material).

overall phenotypic characteristics resulting from the mixture of strains that possessed different properties. Strains 4 and 25 showed a mixture of positive and negative PZase test results, suggesting that these strains might have been deemed positive despite the presence of a PZase-negative strain (15). Strain 25 appeared to be a mixture of a *pncA* mutant and a wild-type strain, and the initial analysis was reflective of a wild-type strain. Shi et al. (16) identified the ribosomal protein S1, encoded by the *rpsA* mutation, as an alternative target of POA that might be associated with PZA resistance in the absence of mutations in *pncA*. Moreover, Sheen et al. (17) reported that the POA efflux rate is associated with PZA resistance. Thus, the six PZA-resistant strains without *pncA* mutations in this study might carry *rpsA* mutations or might have altered POA efflux.

Three strains failed to yield *pncA* PCR amplicons. Strains 33, 47, and 61 produced PCR products at Rv2040 and Rv2047, Rv2041 and Rv2045, and Rv2031 and Rv2046, respectively. Each of these strains carried a complete deletion of *pncA*, which, to the best of our knowledge, is a novel finding. In addition, all three strains had MICs of >1,600 μg/ml. Strains 33, 47, and 61 contained a 4,475-bp deletion from Rv2041 to Rv2046, a 1,565-bp deletion from Rv2042 to Rv2044, and a 6,258-bp deletion from

TABLE 1 Results of retesting isolated strains with divergent results from PZA MIC measurements using the Bactec MGIT 960 system, *pncA* gene sequencing, PZase analysis, and VNTR analysis

	Results for original strain				Results for isolated strain			
Original strain no.	MGIT PZA MIC (μg/ml)	*pncA* mutation	PZase analysis	Isolated strain no.	MGIT PZA MIC (μg/ml)	*pncA* mutation	PZase analysis	VNTR[a]
4	>1,600	G insertion at 392	Positive	i	≤100	None	Positive	Consistent in all loci
				ii	>1,600	G insertion at 392	Negative	
6	400	None	Positive	i	<100	None	Positive	
13	>1600	None	Positive	i	≤100	None	Positive	Consistent in all loci
				ii	>1,600	None	Positive	
17	400	None	Positive	i	≤100	None	Positive	QUB11b:7[b]
				ii	400	None	Positive	QUB11b:6[b]
				iii	800	None	Positive	QUB11b:7[b]
25	800	None	Positive	i	≤100	None	Positive	Consistent in all loci
				ii	400	None	Positive	
				iii	>1,600	T→G at 456, V139G	Negative	
50	200	None	Positive	i	≤100	None	Positive	Consistent in all loci
				ii	400	None	Positive	
79	200	None	Positive	i	≤100	None	Positive	Consistent in all loci
				ii	400	None	Positive	

[a] Compared to results for the isolated strain among the Supply et al. (14) 15-locus VNTR.
[b] Recognized a difference in the copy number at QUB11b.

Rv2037 to Rv2045, respectively (see Fig. S1 in the supplemental material). These results suggest that the entire *pncA* was deleted in *M. tuberculosis*, demonstrating that strains lacking *pncA* can still be PZA resistant.

ACKNOWLEDGMENT

This study was supported by a health science research grant from the Ministry of Health, Welfare, and Labor (H23-Shinko-Ippan-001).

REFERENCES

1. **British Medical Research Council.** 1986. Controlled clinical trial of 4 short-course regimens of chemotherapy (three 6-month and one 8-month) for pulmonary tuberculosis: final report. East and Central African/British Medical Research Council Fifth Collaborative Study. Tubercle **67**:5–15.
2. **Heifets L, Lindholm-Levy P.** 1992. Pyrazinamide sterilizing activity *in vitro* against semidormant *Mycobacterium tuberculosis* bacterial populations. Am. Rev. Respir. Dis. **145**:1223–1225. http://dx.doi.org/10.1164/ajrccm/145.5.1223.
3. **Scorpio A, Zhang Y.** 1996. Mutations in *pncA*, a gene encoding pyrazinamidase/nicotinamidase, cause resistance to the antituberculous drug pyrazinamide in tubercle bacillus. Nat. Med. **2**:662–667. http://dx.doi.org/10.1038/nm0696-662.
4. **Zhang Y, Permar S, Sun Z.** 2002. Conditions that may affect the results of susceptibility testing of *Mycobacterium tuberculosis* to pyrazinamide. J. Med. Microbiol. **51**:42–49.
5. **McDermott W, Tompsett R.** 1954. Activation of pyrazinamide and nicotinamide in acidic environments *in vitro*. Am. Rev. Tuberc. **70**:748–754.
6. **Aono A, Hirano K, Hamasaki S, Abe C.** 2002. Evaluation of BACTEC MGIT 960 PZA medium for susceptibility testing of *Mycobacterium tuberculosis* to pyrazinamide (PZA): compared with the results of pyrazinamidase assay and Kyokuto PZA test. Diagn. Microbiol. Infect. Dis. **44**:347–352. http://dx.doi.org/10.1016/S0732-8893(02)00471-6.
7. **Sekiguchi J, Tomohiko N, Tohru MA, Fumiko K, Intetsu K, Ewa AK, Zofia Z, Koji M, Toshinori S, Hiroshi Y, Seiya K, Toru M, Teruo K.** 2007. Development and evaluation of a line probe assay for rapid identification of *pncA* mutations in pyrazinamide-resistant *Mycobacterium tuberculosis* strains. J. Clin. Microbiol. **45**:2802–2807. http://dx.doi.org/10.1128/JCM.00352-07.
8. **Clinical and Laboratory Standards Institute.** 2012. Susceptibility testing of mycobacteria, nocardiae, and other aerobic actinomycetes; approved standard, 2nd ed. Document M24-A2. Clinical and Laboratory Standards Institute, Wayne, PA.
9. **Louw GE, Warren RM, Donald PR, Murray MB, Bosman M, Van Helden PD, Young DB, Victor TC.** 2006. Frequency and implications of pyrazinamide resistance in managing previously treated tuberculosis patients. Int. J. Tuberc. Lung Dis. **10**:802–807.
10. **Marttila HJ, Marjamaki M, Vyshnevskaya E, Vyshnevskiy BI, Otten TF, Vasilyef AV, Viljanen MK.** 1999. *pncA* mutations in pyrazinamide-resistant *Mycobacterium tuberculosis* isolates from northwestern Russia. Antimicrob. Agents Chemother. **43**:1764–1766.
11. **Werngren J, Sturegård E, Juréen P, Ängeby K, Hoffner S, Schön T.** 2012. Reevaluation of the critical concentration for drug susceptibility testing of *Mycobacterium tuberculosis* against pyrazinamide using wild-type MIC distributions and *pncA* gene sequencing. Antimicrob. Agents Chemother. **56**:1253–1257. http://dx.doi.org/10.1128/AAC.05894-11.
12. **Wayne LG.** 1974. Simple pyrazinamidase and urease tests for routine identification of mycobacteria. Am. Rev. Respir. Dis. **109**:147–151.
13. **Sreevatsan S, Pan X, Zhang Y, Kreiswirth BN, Musser JM.** 1997. Mutations associated with pyrazinamide resistance in *pncA* of *Mycobacterium tuberculosis* complex organisms. Antimicrob. Agents Chemother. **41**:636–640.
14. **Supply P, Allix C, Lesjean S, Cardoso-Oelemann M, Rüsch-Gerdes S, Willery E, Savine E, de Haas P, van Deutekom H, Roring S, Bifani P, Kurepina N, Kreiswirth B, Sola C, Rastogi N, Vatin V, Gutierrez MC, Fauville M, Niemann S, Skuce R, Kremer K, Locht C, Soolingen D.** 2006. Proposal for standardization of optimized mycobacterial interspersed repetitive unit-variable-number tandem repeat typing of *Mycobacterium tuberculosis*. J. Clin. Microbiol. **44**:4498–4510. http://dx.doi.org/10.1128/JCM.01392-06.
15. **McClatchy JK, Tsang AY, Cernich MS.** 1981. Use of pyrazinamidase activity on *Mycobacterium tuberculosis* as a rapid method for determination of pyrazinamide susceptibility. Antimicrob. Agents Chemother. **20**:556–557. http://dx.doi.org/10.1128/AAC.20.4.556.
16. **Shi W, Zhang X, Jiang X, Yuan H, Lee JS, Barry CE III, Wang H, Zhang W, Zhang Y.** 2011. Pyrazinamide inhibits trans-translation in *Mycobacterium tuberculosis*. Science **333**:1630–1632. http://dx.doi.org/10.1126/science.1208813.
17. **Sheen P, Lozano K, Gilman RH, Valencia HJ, Loli S, Fuentes P, Grandjean L, Zimic M.** 2013. *pncA* gene expression and prediction factors on pyrazinamide resistance in *Mycobacterium tuberculosis*. Tuberculosis **93**:515–522. http://dx.doi.org/10.1016/j.tube.2013.03.005.

Journal of Microbiological Methods 101 (2014) 44–48

Contents lists available at ScienceDirect

Journal of Microbiological Methods

journal homepage: www.elsevier.com/locate/jmicmeth

Optimization of the microscopic observation drug susceptibility assay for four first-line drugs using *Mycobacterium tuberculosis* reference strains and clinical isolates

Hiroyuki Nishiyama [a,b,*], Akio Aono [b], Tetsuhiro Sugamoto [a], Kazue Mizuno [c], Kinuyo Chikamatsu [b], Hiroyuki Yamada [b], Satoshi Mitarai [b]

[a] Department of International Cooperation, Japan Anti-Tuberculosis Association, 3-1-24 Matsuyama Kiyose-shi, Tokyo 204-8533, Japan
[b] Department of Mycobacterium Reference and Research, Research Institute of Tuberculosis, Japan Anti-Tuberculosis Association, 3-1-24 Matsuyama Kiyose-shi, Tokyo 204-8533, Japan
[c] Department of Clinical Microbiology, Fukujuji Hospital, Japan Anti-Tuberculosis Association, 3-1-24 Matsuyama Kiyose-shi, Tokyo 204-8533, Japan

ARTICLE INFO

Article history:
Received 17 January 2014
Received in revised form 27 March 2014
Accepted 28 March 2014
Available online 6 April 2014

Keywords:
Drug susceptibility testing
MODS
Smear negative
Turnaround time

ABSTRACT

Objective: The aim of this study is to determine the appropriate cut-off value and turnaround time of the microscopic observation drug susceptibility assay (MODS) for isoniazid (INH), rifampicin (RMP), streptomycin (STR), and ethambutol (EMB).
Design: A total of 39 *Mycobacterium tuberculosis* strains with confirmed drug susceptibility (reference strains) were tested with a range of drug concentrations to determine the optimal cut-off values for INH, RMP, STR, and EMB by MODS. Standard drug susceptibility testing (DST) results were evaluated relative to the Löwenstein–Jensen (L–J) proportion method. Following which, the performance of MODS was evaluated again using 36 sputum samples from patients with tuberculosis (TB) using the cut-off values determined in the aforementioned process.
Results: With 39 reference strains, DST identified the following cut-off values: 0.8 μg/ml INH (sensitivity, 96.0%; specificity, 92.9%), 2.0 μg/ml RMP (sensitivity, 100%; specificity, 95.5%), 4.0 μg/ml STR (sensitivity, 90.5%; specificity, 93.8%), and 4.0 μg/ml EMB (sensitivity, 100%; specificity, 91.7%). When these cut-off values were used to analyze the 36 clinical isolates, the sensitivity and specificity of MODS were 100% and 93.1% for INH, 100% and 93.8% for RMP, 87.5% and 96.4% for STR, and 100% and 88.2% for EMB, respectively. The turnaround time for these clinical specimens was 9.0 days by MODS (95% CI: 5.3–12.7), compared with 11.7 days (95% CI: 9.5–13.9) for smear negative specimens.
Conclusion: Our study identified the optimal cut-off values of the four first-line drugs for MODS based on a wide concentration range. With the optimal cut-off values determined in this study, MODS showed high discriminatory efficiency for DST. This study also demonstrated that MODS is useful for rapid diagnosis of drug-resistant TB even for a smear negative specimen, despite the fact that it generally uses smear positive specimens as direct DST.

1. Introduction

The microscopic observation drug susceptibility assay (MODS) is a high performance assay with a short turnaround time, high sensitivity and specificity, especially for isoniazid (INH) and rifampicin (RMP) (Bwanga et al., 2010; Caviedes et al., 2000; Dixit et al., 2012; Limaye et al., 2010; Makamure et al., 2013; Mello et al., 2007; Mengatto et al., 2006; Moore et al., 2004, 2006; Park et al., 2002; Shiferaw et al., 2007). Because MODS is a simple method that requires only liquid culture and an inverted microscope, operation cost is low. Commercial TB MODS Kit™ (Hardy Diagnostics, Santa Maria, CA USA) is now also available. It simplifies preparation procedure and increases biosafety.

This diagnostic tool is easily implemented in limited resource settings generally associated with high burdens of multidrug-resistant tuberculosis (TB) patients or patients with TB/HIV. However, the above literature reveals that the cut-off values of the major anti-TB drugs determined for MODS were only evaluated using 2 to 4 concentrations: 0.1 and 0.4 μg/ml for INH; 0.5, 1.0, and 2.0 μg/ml for RMP; 2.0 and 6.0 μg/ml for streptomycin (STR); and 2.5, 3.75, 5.0, and 7.5 μg/ml for ethambutol (EMB). Such partial analysis led to inconsistencies between studies. For instance, the MODS user guidelines recommend 0.4 μg/ml as the cut-off value for INH (Coronel et al., 2008), whereas a meta-analysis also using MODS recommended 0.1 μg/ml INH (Minion et al., 2010). Commercial TB MODS Kit™ is an analogous system of what MODS user guideline proposes. Its concentrations are 0.4 μg/ml

* Corresponding author at: International Cooperation, Japan Anti-Tuberculosis Association, 3-1-24 Matsuyama Kiyose-shi, Tokyo 204-8533, Japan. Tel.: +81 42 493 5711; fax: +81 42 492 4600.
E-mail address: hnishiyama1@gmail.com (H. Nishiyama).

http://dx.doi.org/10.1016/j.mimet.2014.03.014
0167-7012/

for INH and 1.0 μg/ml for RMP. Therefore, there is an urgent requirement to determine the optimal cut-off values of these first-line drugs for MODS based on a broad range of concentrations. In addition, evaluation between the turnaround time of direct drug susceptibility testing (DST) by MODS and sputum smear grade is limited (Moore et al., 2004, 2006; Shah et al., 2011).

The objective of this study was to determine the optimal cut-off values of the four first-line drugs (INH, RMP, STR, and EMB) for MODS, and to evaluate the turnaround time of MODS according to the sputum smear grade.

2. Materials and methods

2.1. Bacterial strains and clinical specimens

A total of 39 *Mycobacterium tuberculosis* (MTB) stock strains of known drug susceptibility maintained in our laboratory were used in this study. These strains were selected to include both susceptible and resistant strains for each of the first-line drugs: INH, RMP, STR, and EMB. The DST of all 39 strains was performed by MODS, on the Löwenstein–Jensen (L–J) medium by the proportion method, and using the mycobacterium growth indicator tube anti-mycobacterial susceptibility testing (MGIT AST) kit (Becton Dickinson, Sparks, MD). Each strain was sub-cultured in Middlebrook 7H9 broth (Becton Dickinson, Sparks, MD), and the bacterial suspension was adjusted to McFarland standard 0.5. The suspension was used for subsequent DST.

Thirty-nine sputum specimens were collected from confirmed patients with TB at the Fukujuji hospital from January 2010 to May 2010 for routine examination. Each specimen was digested and decontaminated using N-acetyl-L-cysteine (NALC)-NaOH for 15 min at room temperature. The treated specimen was neutralized with phosphate-buffered saline (PBS; pH 6.8), and then centrifuged at 3000 *g* for 20 min at 4 °C. The supernatant was discarded and the sediment was resuspended in 1 ml of PBS. After adding 7 ml of Middlebrook 7H9 broth, each aliquot was graded by smear microscopy. Direct DST was performed by MODS for each specimen. The recovered MTB isolates were utilized for indirect DST by the L–J proportion method after confirming the MTB complex using immunochromatographic assay (Capilia TB, TOUNS, Numazu, Japan). The laboratory examination was not replicated.

2.2. MODS

A sterile 24-well plate (Falcon, Becton Dickinson, NJ, USA) was used for MODS. The wells were filled with 0.4 ml drug-free Middlebrook 7H9 broth (4 wells) supplemented with polymyxin, amphotericin B, nalidixic acid, trimethoprim, and azlocillin (PANTA), and a concentration range of drug-containing (20 wells) Middlebrook 7H9 broth with PANTA. After inoculating 200 μl of specimens into each well, the final drug concentrations were as follows: 0.05, 0.1, 0.2, 0.4, and 0.8 μg/ml for INH; 0.125, 0.25, 0.5, 1.0, and 2.0 μg/ml for RMP; 1.0, 2.0, 4.0, 8.0, and 16.0 μg/ml for STR; and 0.5, 1.0, 2.0, 4.0, and 8.0 μg/ml for EMB. The concentrations in our study were selected considering those used in the previous MODS studies and those used by MGIT AST because the MODS medium is 7H9 broth. The range of concentrations for INH and RMP was almost comparable to those of previous reports. Those of STR were relatively higher than those used in the previous reports considering the possible relatively high MICs of isolates here in our setting, mainly due to the long use of STR and relatively high proportion of STR resistance. On the other hand, the resistance to EMB is very low in our setting and relatively lower MICs of isolates were expected. The MODS plates were incubated (37.0 °C; 5% CO_2) and inspected under an inverted microscope daily from day 4 to day 15, every other day from day 16 to day 25, and twice a week from day 26 to 40 (Moore et al., 2004, 2006).

2.3. Conventional DST by indirect methods

As aforementioned, the stock reference strains and clinical isolates of MTB were subjected to DST by the L–J proportion method. The concentrations of each first line drug in L–J media were as follows: INH, 0.2 μg/ml; RMP, 40 μg/ml; STR, 4.0 μg/ml; and EMB, 2.0 μg/ml, as recommended by WHO. They were incubated at 37 °C up to 6 weeks with weekly inspection. The same stocked strains were subjected to MGIT AST as well, according to the manufacturer's instruction. Those concentrations were as follows: INH, 0.1 μg/ml; RMP, 1.0 μg/ml; STR, 1.0 μg/ml; and EMB, 5.0 μg/ml. The DST results for each drug were recorded as susceptible or resistant.

2.4. Analysis

The turnaround time of MODS for each drug was defined as the time (days) elapsed from inoculation of the clinical specimens to the positive results in the drug-free well. Sensitivity, specificity, efficiency, and Kappa coefficients were used to determine the optimal cut-off values of MODS compared with the indirect L–J proportion method and MGIT AST methods with stock bacterial strains, and for the evaluation of MODS against the cut-off values obtained with the clinical isolates using the L–J proportion method as reference. The lowest concentration was defined as the appropriate cut-off value if the discrimination power was the same among the concentrations employed for the study, which is compatible with the definition of minimal inhibitory concentration (MIC) that the lowest drug concentration produces complete inhibition of the bacterial growth *in vitro*.

2.5. Ethical considerations

A clinical specimen was collected from each patient for routine examination, and the unused fraction was utilized in this study. An informed consent was obtained from each patient for the use of sputum in research.

3. Results

3.1. Determination of the optimal cut-off values for MODS with reference strains

The DST results obtained by the L–J proportion method identified 25, 17, 23, and 15 strains resistant to INH, RMP, STR, and EMB, respectively. There was no discrepancy between the pre-confirmed and current DST results.

In MODS, 0.8 μg/ml INH had the highest efficiency (agreement) of 0.95 and the highest Kappa coefficient of 0.89 (sensitivity, 96.0%; specificity, 92.9%) compared with DST results by L–J (Fig. 1). With regard to RMP, all concentrations used in this study had high discrimination powers. In particular, 2.0 μg/ml RMP showed the highest efficiency of 0.97, and the highest Kappa coefficient of 0.95 (sensitivity, 100.0%; specificity, 95.5%). STR demonstrated a clear trade-off relation between the highest sensitivity and specificity among the concentrations used. Using 1.0 or 2.0 μg/ml as cut-off value yielded the highest sensitivity (90.9%), but a moderate specificity (87.5%). The highest efficiency (0.92) and Kappa coefficient (0.84) were obtained with 4.0 μg/ml, which was identified as the optimal cut-off value (sensitivity, 90.5%; specificity, 93.8%). With regard to EMB, 8.0 μg/ml showed the highest efficiency (0.97) and highest Kappa coefficient (0.95) (sensitivity, 93.3%; specificity, 100.0%). When MODS was conducted on all 39 referral strains using these optimal cut-off values, we detected 24, 17, 19, and 14 strains resistant to INH, RMP, STR, and EMB, respectively.

The MGIT AST yielded no contamination, but there was no growth for 2 of the 39 strains. Therefore, we analyzed the results from 37 strains. The DST results by MGIT AST identified 23, 20, 19, and 11 strains resistant to INH, RMP, STR, and EMB, respectively. The optimal cut-off

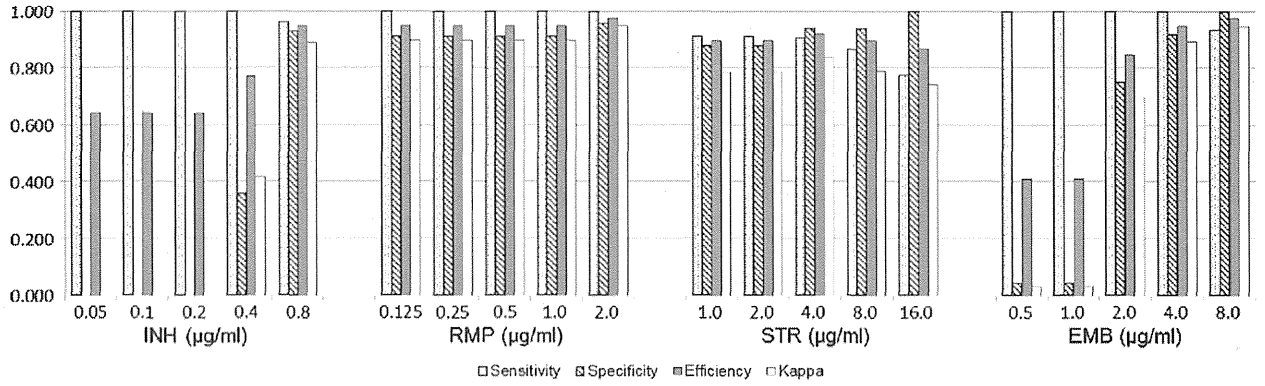

Fig. 1. Performance of MODS compared with the L–J proportion method as a reference by employing the bacterial strains ($n = 39$). Abbreviations: INH, isoniazid; RMP, rifampicin; STR, streptomycin; EMB, ethambutol; Kappa, kappa coefficient; MODS, microscopic observation of drug-susceptibility assay L–J proportion method, Löwenstein–Jensen proportion method.

values for INH and RMP were 0.8 μg/ml and 2.0 μg/ml, respectively, compared with MGIT AST (Fig. 2). In contrast, STR exhibited a trade-off between the highest sensitivity and specificity. But 16.0 μg/ml STR generated the highest efficiency and Kappa coefficient (sensitivity, 78.9%; specificity, 100.0%). For EMB, all concentrations used in this study had poor discrimination powers. The same results were obtained with the L–J proportion method.

3.2. Evaluation of the optimal cut-off values of MODS with clinical sputum specimens

With MODS, there was no contamination, but 3 of the 39 clinical specimens yielded no growth. With the L–J proportion method, all 39 specimens showed growth without contamination. Therefore, 36 specimens were used to assess the performance of MODS using the L–J proportion method as a reference. By the L–J proportion method, DST identified 7, 4, 8, and 2 isolates resistant to INH, RMP, STR, and EMB, respectively.

The highest INH concentration (0.8 μg/ml) demonstrated the highest efficiency (0.94) and Kappa coefficient (0.84) (sensitivity, 100.0%; specificity, 93.1%) (Fig. 3). With regard to RMP, all concentrations generated an efficiency of 0.94 and a Kappa coefficient of 0.77 (sensitivity, 100.0%; specificity, 93.8%). With regard to STR, a cut-off value of 4.0 μg/ml detected resistance with the highest efficiency of 0.94 and the highest Kappa coefficient of 0.84 which is the same discrimination power at 8.0 μg/ml (sensitivity, 87.5%; specificity, 96.4%). With regard to EMB, 4.0 μg/ml and 8.0 μg/ml yielded the highest efficiency (0.89), despite a low Kappa coefficient of 0.46 (sensitivity, 100.0%; specificity, 88.2%). When MODS was conducted on the 36 specimens with these optimal cut-off values, we detected 7, 4, 7, and 2 specimens resistant to INH, RMP, STR, and EMB, respectively.

3.3. Turn-around time of MODS

The average turnaround time for the 36 clinical specimens in MODS was 9.0 days (95% C.I.: 5.3–12.7). According to the sputum smear grade of 36 clinical specimens, the results of DST were obtained after 11.7 days (95% C.I.: 9.5–13.9) for 6 smear negatives, 11.0 days (95% CI: 7.7–14.3) for 4 scanty positives, 7.6 days (95% CI: 5.2–10.0) for 8 of 1+ grade, 9.1 days (95% CI: 5.8–12.4) for 9 of 2+, and 7.6 days (95% CI: 2.4–12.8) for 9 of 3+. Out of 3 no growth among 39 clinical specimens, 2 were smear negatives, and 1 was 1+ grade.

4. Discussion

We identified the most appropriate cut-off for INH by MODS, i.e., 0.8 μg/ml. This result is different from 0.1 μg/ml INH identified by a meta-analysis (Minion et al., 2010), and 0.4 μg/ml INH recommended by the MODS guidelines INH (Coronel et al., 2008). Our result was presumably attributed to the indigenousness of TB strains employed. Considering the diverse drug susceptibility among TB strains, each isolate population may have different MICs. Therefore, further evaluation is needed to reach the consensus that 0.8 μg/ml is the optimal cut-off value for INH based on multiple investigations.

Our study identified 2.0 μg/ml RMP as the most appropriate cut-off value for MODS, which is the same as reported by previous studies (Mello et al., 2007; Moore et al., 2006; Park et al., 2002; Shiferaw et al., 2007). This result suggests that most of the RMP resistant strains are attributed to a single mutation of the *rpoB* gene (Telenti et al., 1993) and show high MIC. Likewise, a study on Japanese patients with TB revealed that most clinical strains resistant to RMP had a *rpoB* gene mutation (Suzuki et al., 1995). This result strongly supports that our

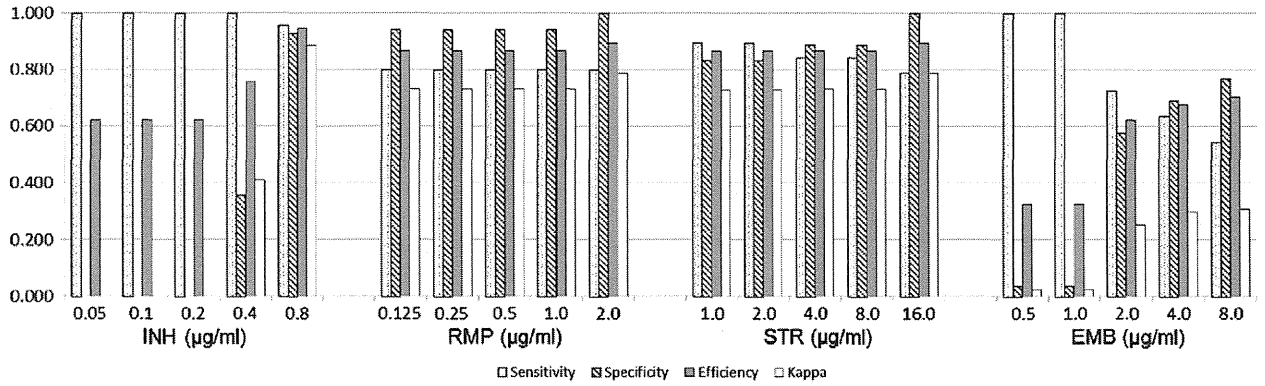

Fig. 2. Performance of MODS compared with MGIT as a reference by employing the bacterial strains ($n = 37$). Abbreviations: INH, isoniazid; RMP, rifampicin; STR, streptomycin; EMB, ethambutol; Kappa, kappa coefficient; MODS, microscopic observation of drug-susceptibility assay; MGIT, mycobacteria growth indicator tube.